NAVAL POSTGRADUATE SCHOOL

MONTEREY, CALIFORNIA

THESIS

MODELING FLOW OVER 3-D WING SPOILERS FOR MODEL B-52

by

Michael A. Palaski

June 2020

Thesis Advisor:	Kevin D. Jones
Co-Advisor:	Vladimir N. Dobrokhodov
Second Reader:	Christopher S. Clay

THIS PAGE INTENTIONALLY LEFT BLANK

REPORT DOCUMENTATION PAGE			*Form Approved OMB No. 0704-0188*

1. AGENCY USE ONLY *(Leave blank)*	**2. REPORT DATE** June 2020	**3. REPORT TYPE AND DATES COVERED** Master's thesis

4. TITLE AND SUBTITLE
MODELING FLOW OVER 3-D WING SPOILERS FOR MODEL B-52

5. FUNDING NUMBERS

6. AUTHOR(S) Michael A. Palaski

7. PERFORMING ORGANIZATION NAME(S) AND ADDRESS(ES)
Naval Postgraduate School
Monterey, CA 93943-5000

8. PERFORMING ORGANIZATION REPORT NUMBER

9. SPONSORING / MONITORING AGENCY NAME(S) AND ADDRESS(ES)
N/A

10. SPONSORING / MONITORING AGENCY REPORT NUMBER

11. SUPPLEMENTARY NOTES The views expressed in this thesis are those of the author and do not reflect the official policy or position of the Department of Defense or the U.S. Government.

12a. DISTRIBUTION / AVAILABILITY STATEMENT
Approved for public release. Distribution is unlimited.

12b. DISTRIBUTION CODE
A

13. ABSTRACT (maximum 200 words)

Analyzation of flight vehicles using computational tools typically relies on a linear model of the aircraft control surfaces to calculate control derivatives and flight response. This information is used to inform the design of simulations and autopilot controls. However, some aircraft implement control surfaces are not well described by linear models, such as asymmetrically employed wing spoilers. This study aims to capture the non-linearity of wing spoilers for use on a 1/18th scale model B-52H through the use of the computational fluid dynamics software ANSYS/CFX. This study models the lift, drag, and moment responses of the wing spoilers at various spoiler angles and angles of attack. This study found that the response of the spoiler was linear from no deployment to half deployment, and beyond this point, the response was non-linear. Continuing research should be conducted to more accurately predict the exact transition point.

14. SUBJECT TERMS CFD, B-52, flow modeling, control surfaces, spoiler	**15. NUMBER OF PAGES** 73
	16. PRICE CODE

17. SECURITY CLASSIFICATION OF REPORT	**18. SECURITY CLASSIFICATION OF THIS PAGE**	**19. SECURITY CLASSIFICATION OF ABSTRACT**	**20. LIMITATION OF ABSTRACT**
Unclassified	Unclassified	Unclassified	UU

NSN 7540-01-280-5500

Standard Form 298 (Rev. 2-89)
Prescribed by ANSI Std. 239-18

THIS PAGE INTENTIONALLY LEFT BLANK

Approved for public release. Distribution is unlimited.

MODELING FLOW OVER 3-D WING SPOILERS FOR MODEL B-52

Michael A. Palaski
Ensign, United States Navy
BS, U.S. Naval Academy, 2019

Submitted in partial fulfillment of the
requirements for the degree of

MASTER OF SCIENCE IN ENGINEERING SCIENCE
(AEROSPACE ENGINEERING)

from the

NAVAL POSTGRADUATE SCHOOL
June 2020

Approved by: Kevin D. Jones
Advisor

Vladimir N. Dobrokhodov
Co-Advisor

Christopher S. Clay
Second Reader

Garth V. Hobson
Chair, Department of Mechanical and Aerospace Engineering

THIS PAGE INTENTIONALLY LEFT BLANK

ABSTRACT

Analyzation of flight vehicles using computational tools typically relies on a linear model of the aircraft control surfaces to calculate control derivatives and flight response. This information is used to inform the design of simulations and autopilot controls. However, some aircraft implement control surfaces are not well described by linear models, such as asymmetrically employed wing spoilers. This study aims to capture the non-linearity of wing spoilers for use on a 1/18th scale model B-52H through the use of the computational fluid dynamics software ANSYS/CFX. This study models the lift, drag, and moment responses of the wing spoilers at various spoiler angles and angles of attack. This study found that the response of the spoiler was linear from no deployment to half deployment, and beyond this point, the response was non-linear. Continuing research should be conducted to more accurately predict the exact transition point.

THIS PAGE INTENTIONALLY LEFT BLANK

TABLE OF CONTENTS

LIST OF FIGURES

LIST OF TABLES

THIS PAGE INTENTIONALLY LEFT BLANK

LIST OF ACRONYMS AND ABBREVIATIONS

2-D	two-dimensional
3-D	three-dimensional
A	planform area
AoA	angle of attack
c	chord length
C_D	drag coefficient
C_L	lift coefficient
C_M	pitching moment coefficient
C_p	pressure coefficient
CAD	computer aided design
CFD	computational fluid dynamics
COP	center of pressure
D	drag force
F_i	force in the i-direction
FVM	finite volume method
L	lift force
p	local pressure
p_∞	free-stream pressure
s	span length
U_∞	free-stream velocity
y+	y-plus (non-dimensional length)
ρ	fluid density
τ_i	torque about the i-axis

THIS PAGE INTENTIONALLY LEFT BLANK

ACKNOWLEDGMENTS

I am forever grateful to my parents for their constant love and encouragement. Without their guidance, I would not be where I am today.

I would like to thank the United States Navy, and particularly those involved in the Shoemaker Scholarship program, for providing me with this wonderful opportunity to attend NPS. Graduate school has always been a dream of mine, and I am thankful for ability to realize this dream so early in my career.

The accomplishment of this research is due to the advice and guidance of Doctor Kevin Jones, Doctor Vladimir Dobrokhodov, and Christopher Clay. Without their shared wisdom, this thesis would not be complete.

THIS PAGE INTENTIONALLY LEFT BLANK

I. INTRODUCTION

The goal of this thesis is to employ the use of commercially available computational fluid dynamics (CFD) software to model the flow over a wing spoiler of a $1/18^{th}$ scale model B-52 Stratofortress. The collected data will be used to inform the design of an autopilot that will provide autonomous control to the model while in flight. This study will provide a starting point that will aid in the preliminary testing of the airframe.

The model B-52 is being developed as a case study on a rapid prototyping process. The end goal of this project is to create a curriculum that will walk students through the design process to create their own such designs.

For most unmanned aerial vehicles (UAVs) with traditional control surfaces, the design is relatively simple. These control surfaces operate in predictable, linear regimes. However, the nature of a wing spoiler is highly non-linear. Due to the high complexity of this fluid flows, CFD provides an invaluable resource to model and analyze flows at low cost and in relative short order. This is accomplished by dividing the fluid domain into small sections using a technique known as Finite Volume Method (FVM). The fluid properties for each small volume are determined based on those around it using the Navier-Stokes equations.

A. MOTIVATION

The objective of this thesis is to observe the fluid effect of a wing spoiler at low speeds and determine the relationship between deployment angle and lift and drag forces. CFD processes will be used to determine characteristic values of the wing at various spoiler angles and incident flow angles. These values will be implemented in the design of an autopilot. Generally, autopilots operate under the assumption that the change in forces vary linearly with control surface deflection. However, the fluid effect that a spoiler creates in inherently non-linear. Therefore, it is important to investigate this affect, and either confirm a linear fit, or some other non-linear parametric fit, that describes the spoilers affect in order to implement this into a controller.

B. GOALS OF THE B-52 PROJECT

The goal of the project is to create an airworthy model using rapid-prototyping additive manufacturing techniques, such as three-dimensional (3-D) printing. This allows for the model to pass through many design-build-test iterations in a short amount of time. It also allows for quick replacement of damaged parts. Materials for this type of design also tend to be more cost-effective than those used in more traditional manufacturing processes.

The model is intended to be flown using an autopilot that will control it throughout all phases of flight. The code used to control this autopilot is being developed by Ben Hogin [1].

At the conclusion of the project, the rapid prototyping process is to be codified into a curriculum that will walk students through the steps of creating their own models in a similar fashion. Short lecture videos will provide guidance through the phases of iterative design, manufacture, testing, and analysis.

C. GOALS OF THE SPOILER ANALYSIS

The objective of this thesis is to predict the non-linear effects of a wing spoiler at flight speed of a $1/18^{th}$ scale model B-52. The analysis is meant to provide an accurate model to give a prediction of flight performance to the pilot and to inform design of the autopilot. The secondary goal of this thesis is to provide an example of CFD implementation to be used in the creation of educational content.

D. BACKGROUND

The B-52 Stratofortress is a long-range bomber employed by the United States Air Force, beginning service in 1955 [2]. The airframe has an enormous wingspan, which causes the wings to flex greatly under their own weight. During flight, the wings to flex upward and twist under aerodynamic forces. The use of traditional ailerons would place significant torsional stress on the frame during rolling maneuvers. This torsional stress causes wingtips to twist, in effect changing the local angle of attack (AoA). If the aileron

is deflected down, the wing will twist such that the local AoA is decreased, decreasing the total lift.

Aileron is also a concern near landing when the aircraft is operating at low speed and high AoA. Deflecting an aileron down affects the local flow around the wing and raises the local AoA. Because the wing is already operating near stall conditions, this increase in AoA exceeds that maximum lift AoA and causes the wing to stall and lose lift.

In both cases, lift is decreased instead of increased, and a left roll input may cause a roll to the right. The implementation of spoilers solves both of these problems, and so this system of control was chosen for use on the B-52 [3].

The spoilers also function to reduce lift and increase drag. In most landing cases, the B-52 will use its spoilers symmetrically [4]. Its large wingspan and flaps give the airframe a glider-like characteristic. The wings are creating so much lift, that the spoilers are needed to diminish lift in order to land. This is done by depleting the aircraft's kinetic and potential energy. The drag caused by the spoiler reduces the kinetic energy, and the loss of lift causes the aircraft to drop in altitude, decreasing potential energy. Thus, it is important to quantify how much the lift and drag forces change when deploying the spoilers. CFD provides an inexpensive and time saving way to model these complex flows.

CFD functions by first creating a Computer aided design (CAD) model of the volume in which the fluid will move. This solid model is then imported into the mesher, software responsible for dividing the large fluid domain into small volumes. For each volume, the conservation laws of mass, momentum, and energy are used to estimate the conditions in the volume of interest based on the conditions in the other bordering volumes. These calculations must be done iteratively, as there is no closed form solution to the governing equations. Iterations are performed until a specified threshold of residual error (typically just 'residuals') has been reached. Once the residuals become constant (to within a small threshold) between iterations, the calculation is deemed to be converged and results can be viewed and post-processed [5]. For simple flows and low-cost applications, CFD studies may not be warranted. However, as the cost of the system or flow complexity

increases, and high-fidelity predictions are necessary, CFD is much preferred to creating and testing scale prototypes.

For this reason, CFD plays a large part in the realm of aerospace design. If a design can be tested and fine-tuned in a simulated environment, then the first physical model will likely be close to meeting design specifications, requiring fewer physical changes to be made.

E. THESIS OUTLINE

The following parts of the thesis follow the development and testing of different CFD models of the wing.

Analysis of a 2-D model of the wing airfoil is described in Chapters II and III. For this test, the spoiler was not considered. Aerodynamic characteristics of the airfoil at low speeds were required to properly model the aircraft in a virtual environment for testing of the autopilot. This also provided a starting point for analysis of the full wing.

Development of a 3-D model of the wing, including the spoiler, are covered in Chapters IV and V. The wing is tested at multiple angles of spoiler deployment at various angles of attack.

Conclusions and recommendations for future work can be found in Chapter VI.

II. MODELING OF A 2-D REPRESENTATIVE AIRFOIL

This portion of the study aims to use ANSYS CFX in order to calculate the critical parameters of the airfoil used on the model B-52. These values will be input into a computer model of the B-52 in order to calculate the stability derivatives of the control surfaces. The stability derivatives will inform the model's autopilot on the proper positioning of control surfaces on the model to ensure stable, coordinated flight.

A. AUTOPILOT

The autopilot code to be used in this model was developed by Ben Hogin [1]. In designing this code, a flight model of the airframe was constructed using MachUp, a free cloud-based aerodynamic modeling tool. This program requires input parameters that describe the performance of the airfoil shape. These parameters are zero lift AoA, maximum lift coefficient, $C_{L_{MAX}}$, moment coefficient, C_M, at zero lift AoA, drag coefficient, C_D, at zero lift AoA, slope of the coefficients of moment and lift plots, and quadratic fit for the drag polar. These values were calculated by testing the two-dimensional (2-D) airfoil at various AoAs using CFD. The final values of these parameters are given in the results section in Chapter III.

B. CFD TESTING

1. Geometry

Testing was conducted on a mid-span section taken from the 3-D model of the B-52 wing. This section is similar to a NACA 63A210 airfoil, which was used in designing the 3-D wing model. The section, shown in Figure 1, was provided by Dr. Kevin Jones [6]. It is important to note that the chord of the airfoil sits at a five-degree angle with respect to the axes in the CAD drawing. For analysis of this model, the AoA presented is the true AoA with respect to the chord, unless otherwise noted. The chord length of this section is 0.367 m.

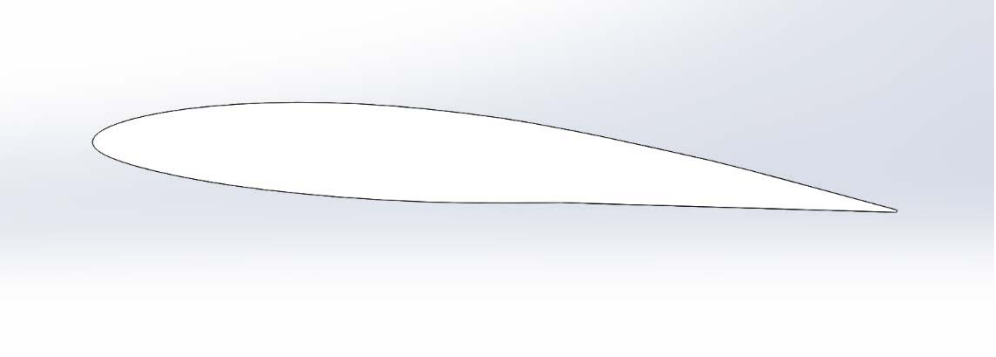

Figure 1. Mid-span section of model B-52 wing. Source: [6].

The coordinates were converted to a sketch within SolidWorks. The ANSYS CFX solver requires a 3-D body as a geometry input, so a thin solid was created by drawing a rectangle around the airfoil and extruding to a thickness of 1 mm. The edges of the fluid domain were drawn a distance of 10 chord lengths from the airfoil. This space ensures that the influence of the boundaries does not affect the calculation on the surface of the airfoil. The final solid is shown in Figure 2.

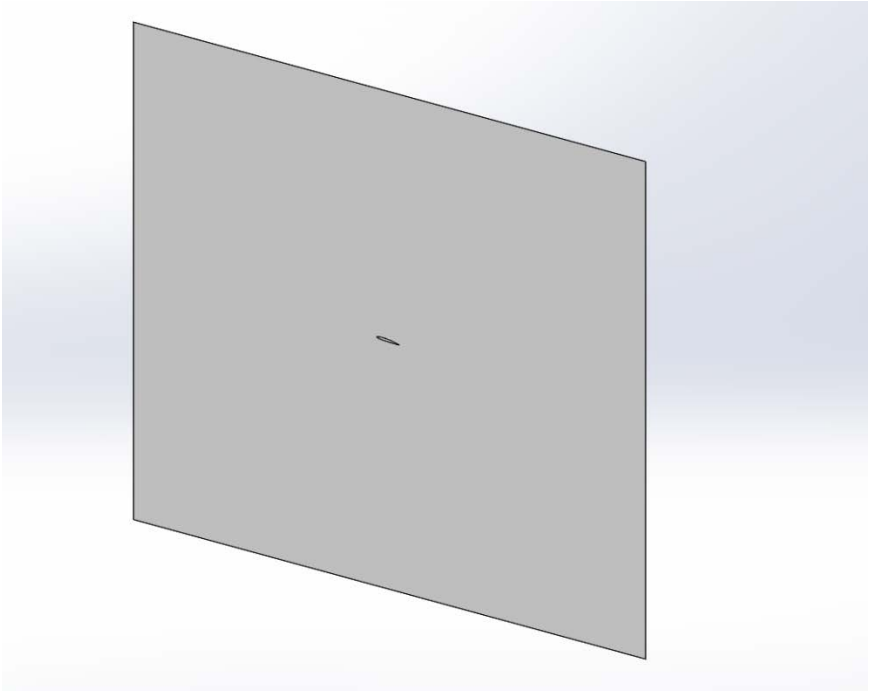

Figure 2. Fluid domain geometry for 2-D airfoil test

2. Mesh

This geometry was imported into the ANSYS Meshing tool. A sweep method was used to create the mesh, in which the mesh cells created perpendicular to the side faces. Sweeping allows the 3-D geometry to be calculated as closely as possible to a true 2-D study within the environment of the CFX solver. CFX is inherently a 3-D solver, and thus requires a 3-D model to conduct a calculation. The sweep method is used to create mesh that is only one volume division wide, so there is no flow calculation normal to the large side planes.

In order to capture the flow effects at the surface of the wing within the boundary layer, an inflation layer was created around the airfoil. The inflation layer is a tool used to insert many points close to a surface. In most of the fluid domain, gradients are fairly small, but near to surfaces these gradients become significant. Gradients are best resolved when there are many mesh points in the area, and the inflation layer provides these points by creating layers of points normal to a surface. Inflation layers also are meant to provide an orthogonal structure to the mesh. Most turbulence transition models assume that the points in the mesh are orthogonal, so a properly structured mesh will predict turbulent transition more accurately.

Insertion of the inflation layer was done by selecting the symmetry face as the geometry, and the edge of the airfoil on that face as the boundary. This tells the mesher to create a 2-D mesh on the front face, and then use the sweep method to mirror this mesh on the back face, creating a mesh one volume wide in the third direction.

In evaluating the inflation layer, one important parameter is the y+ value. This value is a dimensionless distance that is related to the shear stress on the wing surface. It is used to measure distance from the wing surface in boundary layer flow. Since it is non-dimensional, it is not specific to any particular boundary layer conditions, and can be used in the measurement of any boundary layer.

When investigating turbulent boundary layers, the boundary layer can be divided into three distinct regions based on the fluid behavior. These regions can be loosely delineated by their distance from the surface, as described by the y+ value. Fluid friction

on the wing is based on the fluid flow characteristics within the closest layer of the turbulent boundary layer, the laminar sublayer, which is made up of the fluid in direct contact with the wing surface. Generally, this region of the boundary layer extends to a y+ value of about 5-7 [7].

To correctly predict drag and capture the fluid behavior in the laminar sublayer, it is important to have about five mesh points present within the laminar sublayer. The mesher uses a geometric progression to place these points, so it is common practice to keep the y+ value of the first mesh point above the surface at about 1. This ensures that about five points will be inserted below a y+ distance of 7. When the y+ is plotted, the y+ value of the first point is displayed on the surface, as shown in Figure 3. If the value of y+ is greater than 1, then the distance from the surface to the first mesh point should be made smaller, and vice versa.

The y+ value is most important in areas where turbulent flow is predicted. The transition from laminar to turbulent flow depends on the distance from the stagnation point that the flow has traveled, so the value of y+ near the stagnation point is less important than on the upper and lower surfaces of the wing.

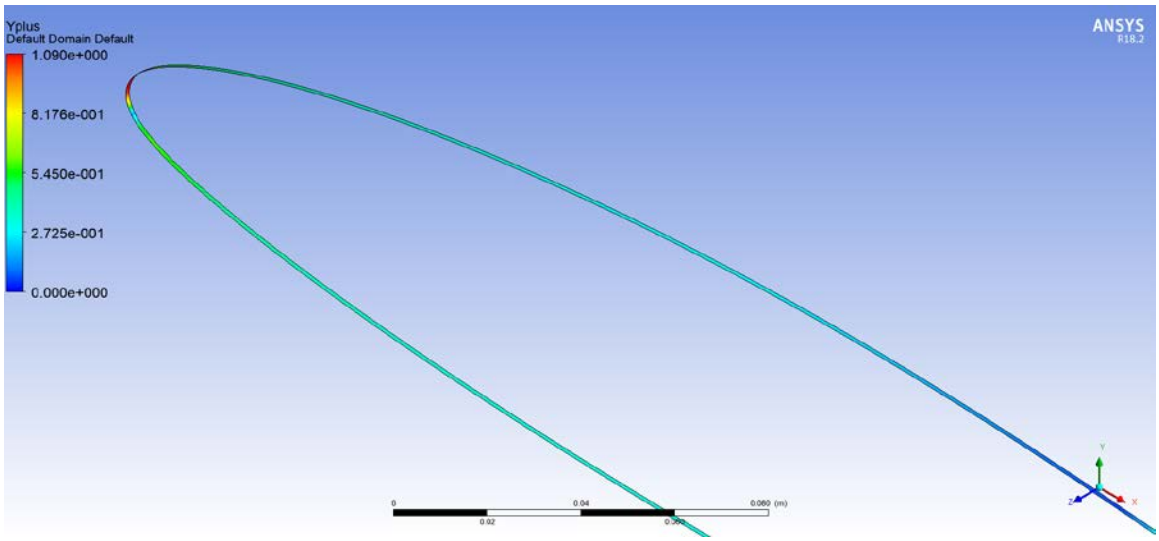

Figure 3. Y-plus values on airfoil surface

An edge sizing restriction was also used to create a large amount of points surrounding the leading and trailing edges of the airfoil. These are areas of great interest due to the rapidly changing fluid properties. It is important to insert enough mesh points in these areas to capture the large gradients in pressure and velocity. The leading edge and trailing edge meshes are shown in Figure 4.

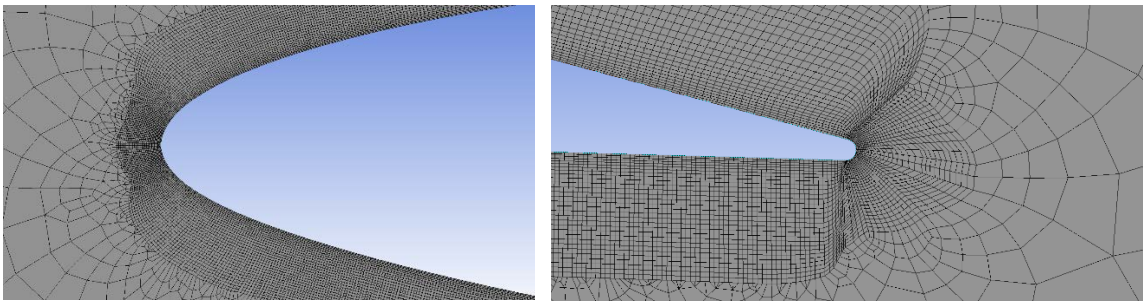

Figure 4. Leading edge (left) and trailing edge (right) meshes

The final mesh is shown in Figure 5. The pictured mesh contains about 30,000 nodes. The characteristics of the inflation layer and edge sizing restriction are given in Appendix A.

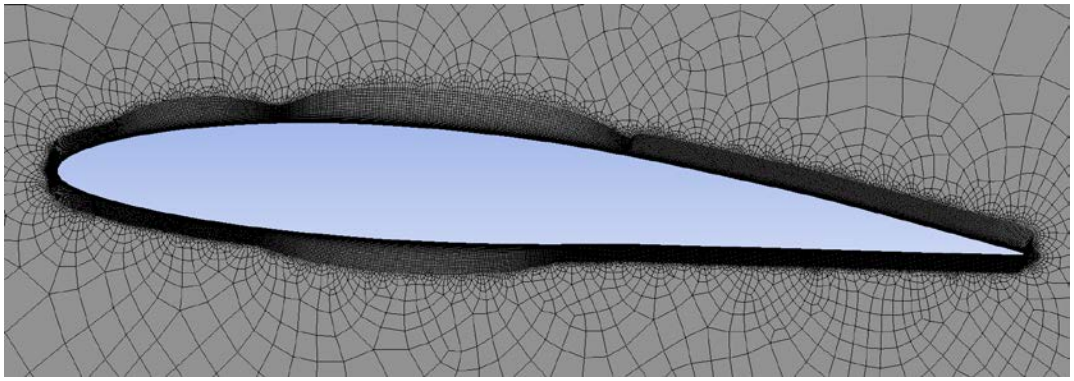

Figure 5. 2-D airfoil mesh

3. Setup

The calculation was initialized in the ANSYS CFX-Pre module. The initial test was conducted with a zero AoA input with respect to the fluid domain axes, or 5° AoA with respect to the chord. The inlet was given a normal flow velocity of 25 m/s. For air at 25°C and a chord of 0.367 m, this correlates to a Reynolds number of 612,000. This velocity would be used for each subsequent test, as it is an approximate airspeed of the model B-52. The outlet was set to zero ambient pressure. The large side walls were set as symmetry boundaries, to mirror the flow around the airfoil that would normally extend from this quasi-2-D section. For the zero AoA test, the top and bottom were set as openings, to allow flow into and out of the domain.

In order to change the incident AoA on the wing, the conditions on the top and bottom surfaces were changed. For a positive AoA, both the inlet and bottom surfaces were initialized as inlets using Cartesian coordinate velocity components. An image of this setup is shown in Figure 6. For negative AoA, the same process was completed for the inlet and top surfaces. To facilitate easy change in AoA (and flow velocity, if necessary), the velocity components were coded using the ANSYS expression language. An example of these variable definitions is shown in Table 1.

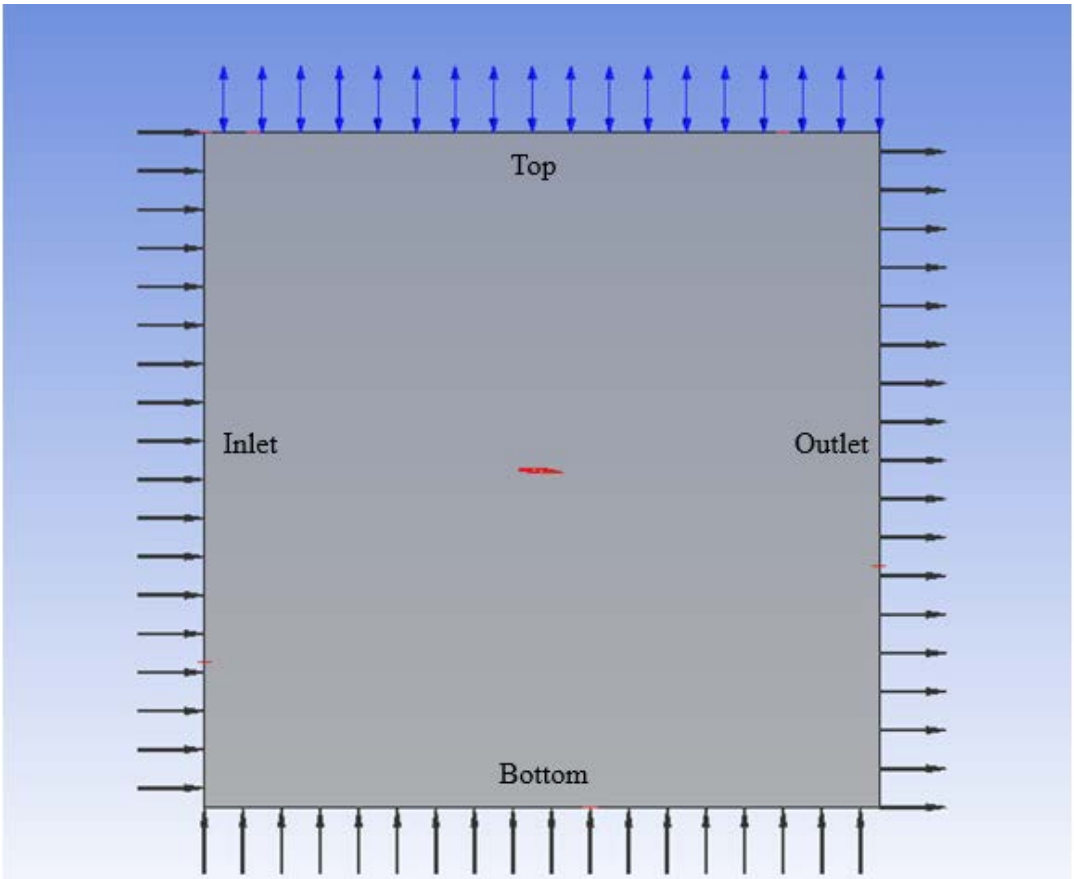

Figure 6. Boundary conditions for positive AoA

Table 1. Flow velocity and angle parameter definitions

Parameter	**Variable**	**Expression**
Normal Flow Velocity	bigU	25 [m/s]
AoA	AoA	5 [deg]
x-velocity component	littleU	bigU*cos(AoA)
y-velocity component	littleV	bigU*sin(AoA)

Because of the five-degree angle of the airfoil chord, an AoA of negative five degrees programed into the CFD calculation would correlate to a zero AoA with respect to the chord. Thus, five degrees was added to the input AoA value to obtain the true AoA value.

A Shear Stress Transport turbulence model was used in this analysis, with a gamma-theta model used for transition. This model is used in this simulation because of its accurate prediction of flow separation onset, an important factor in low speed flows. It also provides accurate drag prediction in flows that experience natural transition [5].

4. Solution

This information was sent to the solver module. The governing equations were solved for each element during each iteration. The calculation was allowed to iterate until the residual errors reached a constant value. This process was completed for tests at multiple AoA. A sample plot of the mass/momentum residuals over the course of the calculation is shown in Figure 7. It is important to ensure convergence in both mass/momentum and turbulence residuals, as one may reach convergence before the other. Both sets of residuals must be converged to provide the most accurate solution. The calculation in Figure 7 was allowed to continue to run after the mass/momentum residuals converged until the for turbulence residuals (not pictured) converged.

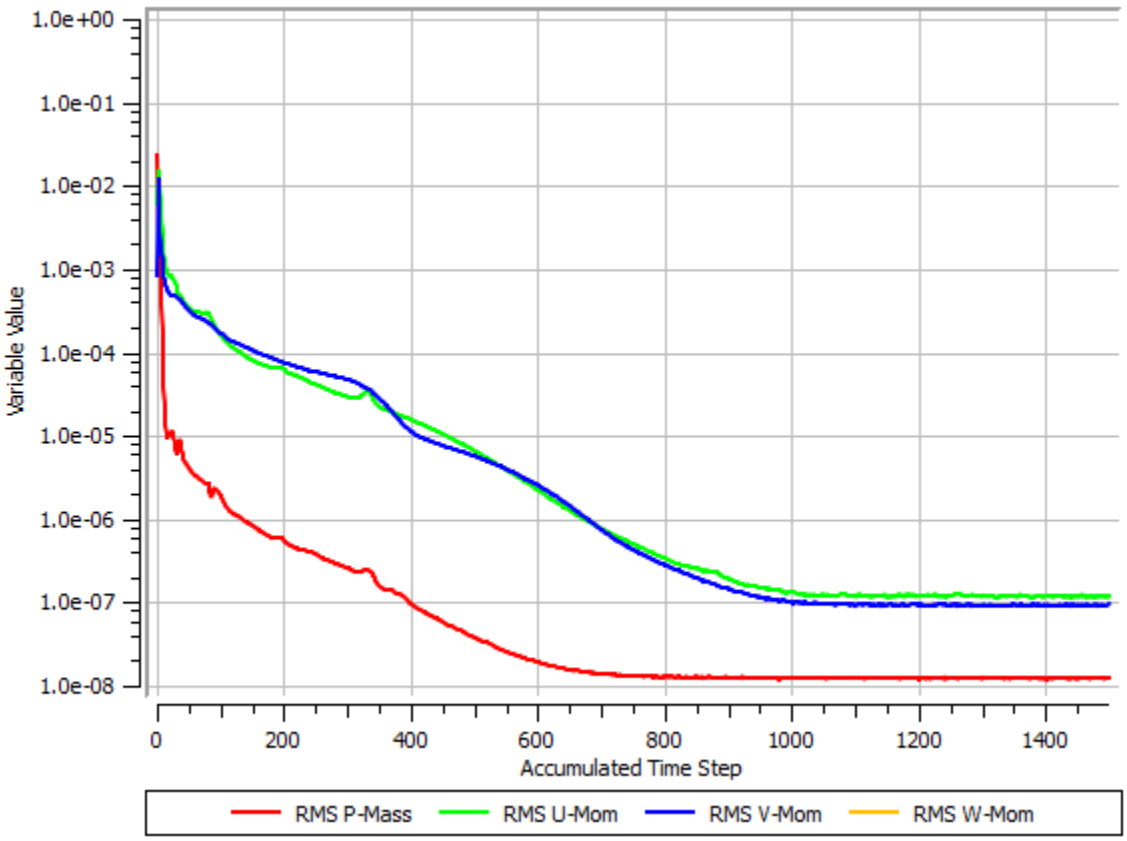

Figure 7. Example residual plot

After completing each calculation, the results were compiled into a single file directory for ease of processing data. Namely, a list of the x-direction force, y-direction force, and z-direction torque (pitching moment) was recorded in a spreadsheet. A table of this data is given in Appendix B.

THIS PAGE INTENTIONALLY LEFT BLANK

III. DATA ANALYSIS FOR 2-D AIRFOIL

A. DATA COLLECTION

After a solution was reached, the results were viewed using the CFX-Post module. This was used to calculate lift, drag, and torque information that would be used to calculate coefficients of lift, drag and pitching moment. It was also used to produce velocity and pressure plots around the airfoil.

1. Lift, Drag, and Pitching Moment

To calculate lift, *L*, and drag, *D*, the CFX-Post module internal function calculator was used to calculate forces on the wing in the x- and y-directions, F_x and F_y. These vectors are not the lift and drag, but can be easily rotated to calculate these forces. Again, for this test the wing sits at a five-degree angle. This additional five degrees was subtracted from the input AoA before performing the vector rotation. The vector rotation is done using the following equation.

$$\begin{bmatrix} L \\ D \end{bmatrix} = \begin{bmatrix} \cos(AoA) & -\sin(AoA) \\ \sin(AoA) & \cos(AoA) \end{bmatrix} \begin{bmatrix} F_x \\ F_y \end{bmatrix} \tag{1}$$

Pitching moment is calculated using the function calculator to find the torque about the z-axis, τ_z. This vector represents the pitching moment of the airfoil. This value is calculated about the leading edge of the airfoil.

$$C_M = \tau_z \tag{2}$$

2. Dynamic Pressure

The dynamic pressure, *q*, was calculated using the ANSYS expression language. The values of velocity and density were sampled at the inlet. The expression used to calculate this is shown in equation 3, with the ANSYS expression in Equation 4.

$$q = \frac{\rho U_{\infty}^{2}}{2} \tag{3}$$

$$areaAve(0.5 * Density * Velocity \wedge 2) @ inlet \tag{4}$$

The dynamic pressure is used to normalize the lift, drag, and moment values to determine their non-dimensional coefficients, as shown in equations 5-8.

$$C_P = \frac{p - p_{\infty}}{q} \tag{5}$$

$$C_L = \frac{L}{qA} \tag{6}$$

$$C_D = \frac{D}{qA} \tag{7}$$

$$C_M = \frac{M}{qAc} \tag{8}$$

In these equations, *c* represents the chord, *s* represents the span, *A* represents the product $s \cdot c$, the planform area, and *p* and p_{∞} are the local and free stream pressures, respectively. For this model, the chord length was 0.3670 m and the span was 0.001 m. The calculation of lift, drag, moment, and their associated coefficients are given in Appendix B.

B. ANALYSIS

1. Boundary Layer

Figure 8 shows selected features of the boundary layer around the airfoil at 5° AoA. Near the leading edge, the flow is laminar. This continues until the flow separates, just past the widest part of the airfoil. A separation bubble forms here in the adverse pressure gradient, where pressure rises in the flow direction. Separation triggers the transition from laminar to turbulent flow, which reenergizes the flow, and causes it to reattach to the airfoil.

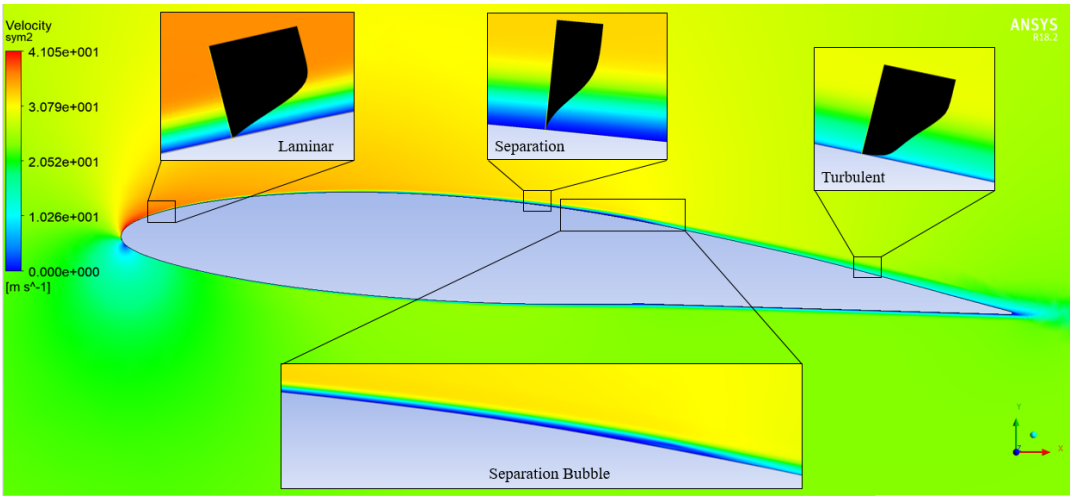

Figure 8. Boundary layer features

2. Pressure Coefficient

The pressure coefficient is a normalized pressure at each point on the surface of the airfoil. If the pressure coefficient is integrated with respect to position, the lift coefficient is obtained. Figure 9 shows a pressure coefficient plot at a 5° AoA (with respect to chord). The top half of the plot represents the suction side of the airfoil, and the bottom shows the pressure side. The lower peak shows the stagnation point. The bump in the upper half shows the position of the separation bubble.

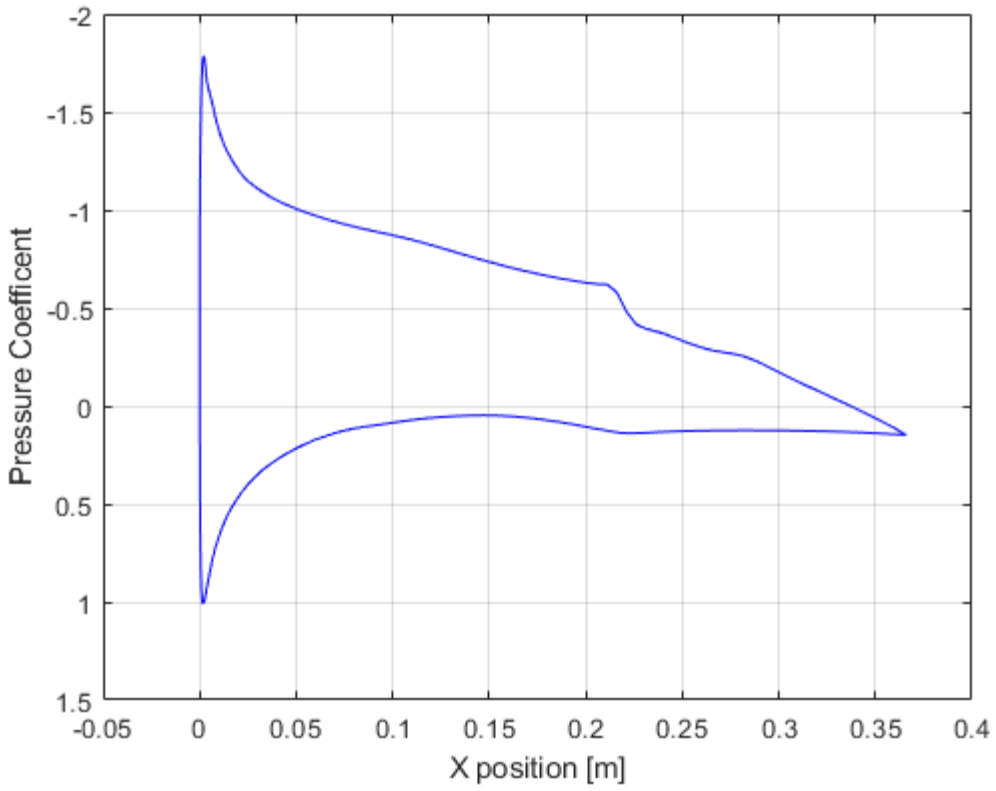

Figure 9. Pressure coefficient for airfoil at 5° AoA

3. X-Wall Shear Stress

The x-wall shear stress is a measure of the frictional shear stress on the surface of the airfoil. While not equal to total drag, integrating this value with respect to position yields the friction drag. Figure 10 shows an x-wall shear stress plot at a 5° AoA (with respect to chord). The stagnation point occurs where the lower line crosses zero after reaching its minimum. The negative wall shear here comes from the back flow around the leading edge of the wing from stagnation to the upper surface. The small section just after 0.2 meters where the plot dips below zero shows the separation bubble. Downstream, a negative wall shear comes from flow in the negative x-direction, indicating a recirculation bubble has formed, caused by the separated flow.

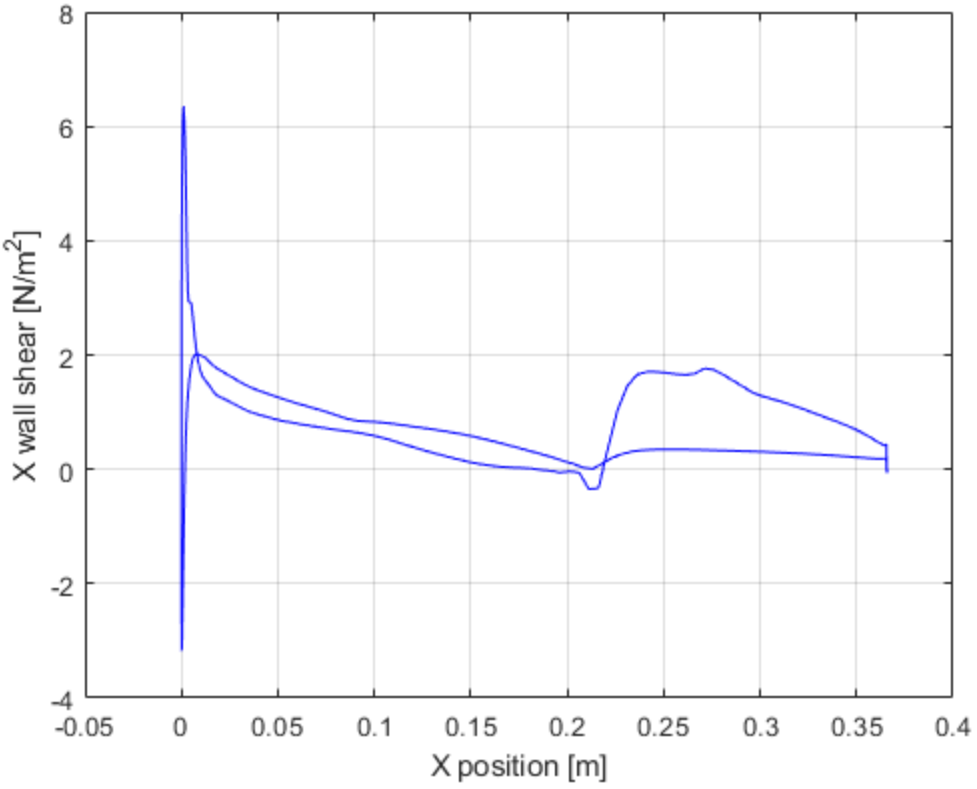

Figure 10. X-wall shear stress for airfoil at 5° AoA

4. Lift Curve

Analysis of the data was conducted using MATLAB's curve fitting tools. The lift coefficient is plotted against AoA in Figure 11. In Figure 11, as with Figure 12 and Figure 13, the AoA is taken with respect to the chord, removing the influence of the 5° built in AoA.

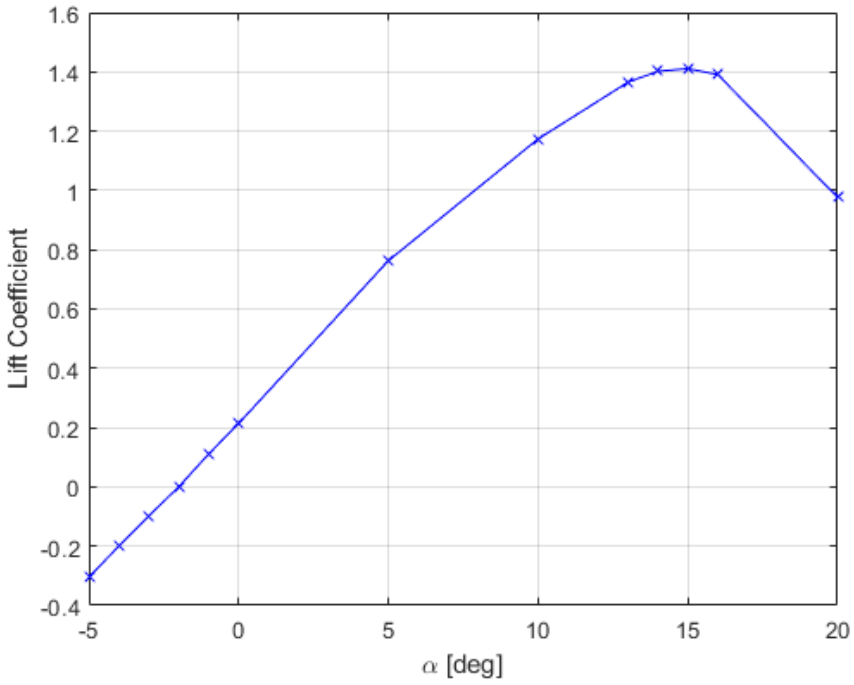

Figure 11. Lift curve for B-52 airfoil

From this plot, values for the lift curve slope, the zero-lift AoA, and maximum lift coefficient were derived. The lift curve slope was calculated by performing a linear regression on the first nine points (before the plot begins to peak). The zero-lift AoA was calculated by interpolating the regression for a corresponding lift coefficient of zero. The maximum lift coefficient was taken as the highest point on the plot. Values for these airfoil parameters are found in Table 2.

5. Moment Curve

The moment coefficient is plotted against AoA in Figure 12. Here, the moment is calculated about the leading edge of the airfoil.

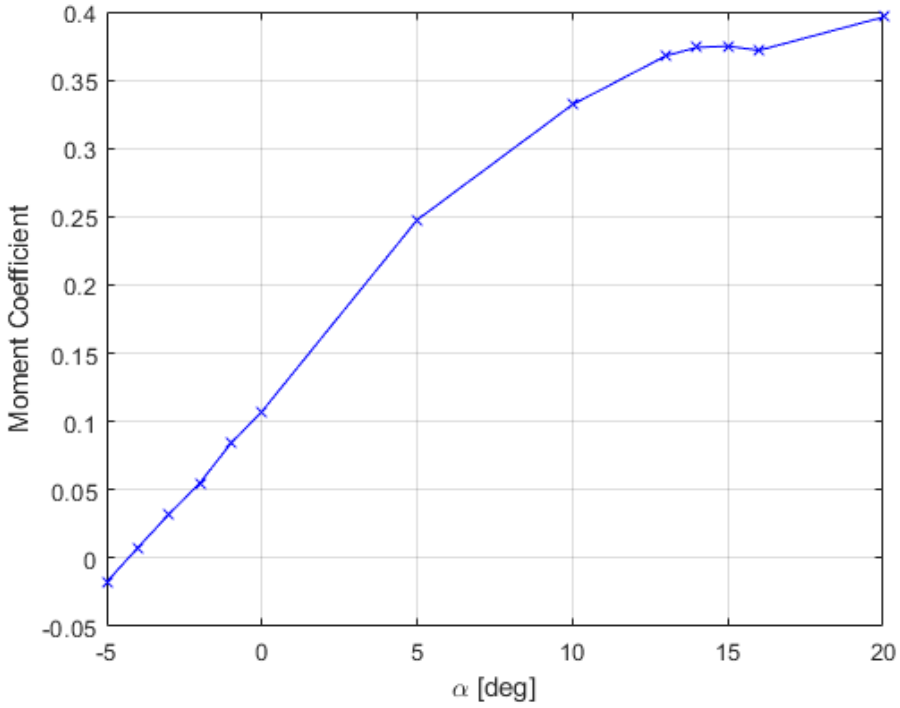

Figure 12. Moment curve for B-52 airfoil

From this plot, values for the moment curve slope and the zero-lift moment coefficient were derived. The moment curve slope was calculated by performing a linear regression on the first nine points (before the plot begins to peak). The zero-lift moment was calculated by interpolating the regression at the value of zero-lift AoA found previously. Values for these airfoil parameters are found in Table 2.

6. Drag Polar

The drag polar for the airfoil is shown in Figure 13. This plot shows the relationship between drag and lift on the airfoil. The point at which the curve reaches a minimum shows the operating point where the least drag occurs. This may not be the optimum operating point, as there are points which produce greater lift without increasing the drag significantly.

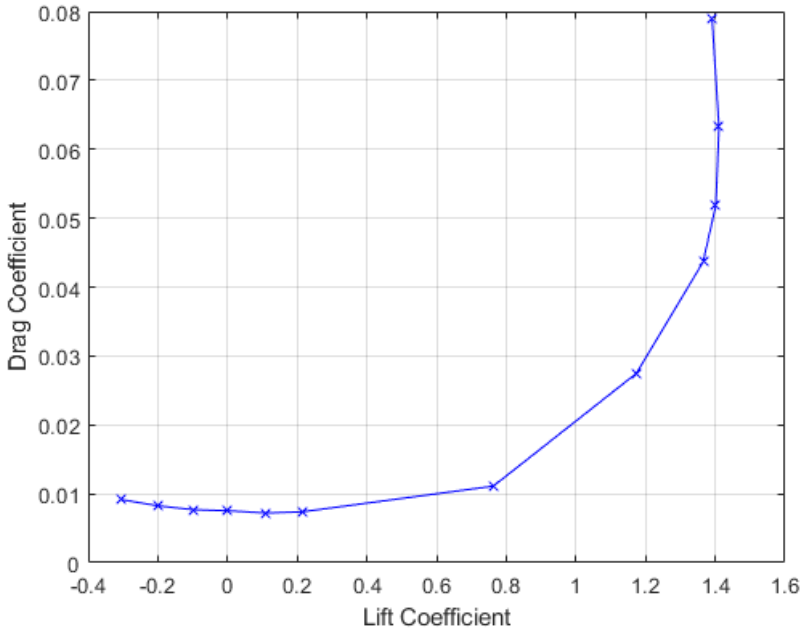

Figure 13. Drag polar for B-52 airfoil

From this plot, values for the drag polar quadratic fit and the zero-lift drag coefficient were derived. A second order polynomial fit was conducted for the first nine points. Beyond the ninth point, the plot cannot be modeled accurately using a quadratic function. This point also marks the beginning of nonlinear behavior on the lift curve plot, and is outside the normal AoA range of operation. The zero-lift drag coefficient was calculated by interpolating this fit at a lift-coefficient value of zero. Values for these airfoil parameters are found in Table 2.

Table 2. 2-D Airfoil Parameters

Parameter	**Value**
Zero-Lift AoA	-0.0350 rad
Lift Curve Slope	3.46e-3 1/rad
Zero-Lift Moment Coefficient	0.0548
Moment Curve Slope	1.79e-3 1/rad
Zero-Lift Drag Coefficient	7.54e-3
Drag Polar Fit, 2nd order Term	-8.89e-3
Drag Polar Fit, 1st order Term	0.0250
Maximum Lift Coefficient	1.41

IV. MODELING OF A 3-D WING WITH SPOILER

A. GEOMETRY

Testing was conducted using a 1/18th scale model of the wing. The half span of the model is 1.566 m in length, but about 0.09 m was lost when the fuselage was removed. The CAD drawing of the wing was provided by Dr. Kevin Jones [8], shown in Figure 14.

This model is not fully accurate to the real B-52, as the coordinates for the airfoil could not be found. A NACA 63A210 airfoil was used as a close match based on photographs of the real aircraft, with 14% thickness at the root and 8% thickness at the tip. The wing also has a 2° washout, where wing is twisted so the tip chord AoA is 2° less than that of the root [4], [9]. For this analysis, the root AoA will be used as the reference. The wing was modeled as closely as possible to the actual B-52, however, due to the large difference in operating Mach number and Reynolds number between the model and the real aircraft, fully replicating the airfoil shape was not deemed essential

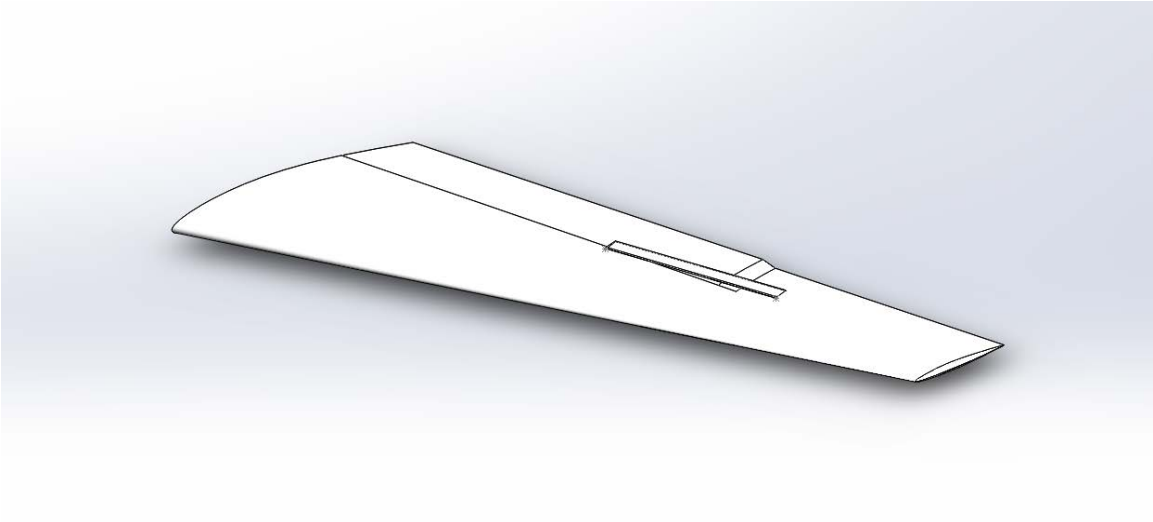

Figure 14. Wing geometry. Source: [8].

The spoiler was then removed from the wing geometry and saved as a separate part file. This allowed the spoiler to be moved independent of the wing when placed in an assembly. The spoiler is shown in Figure 15. It is notably different from that of the real B-52 due to its lack of drag-inducing fingers. However, due to the small scale of this model, modeling of the drag fingers is impractical. Thus, the CFD tests will not account from these features.

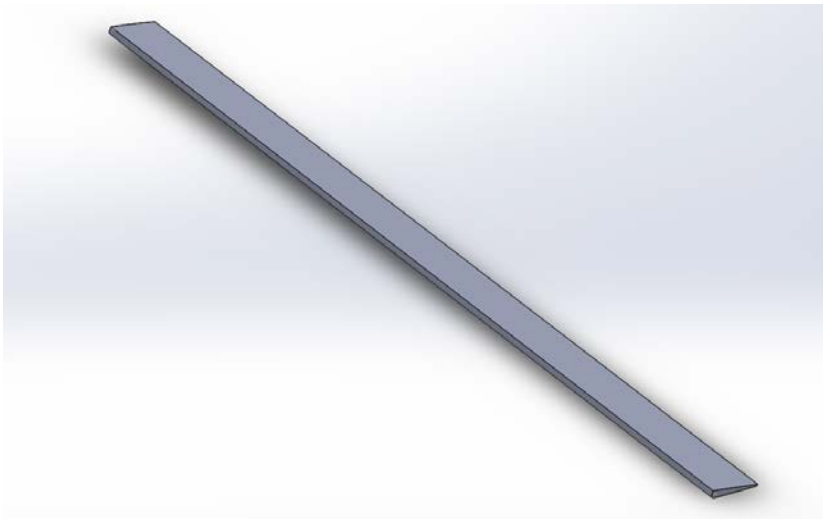

Figure 15. Spoiler geometry

The fluid domain was drawn as a box with dimensions that extend from the wing 10 root chord lengths in all directions. Then the wing and spoiler geometries were removed from the box using the SolidWorks cavity tool. The cavity in which the spoiler resides when not deployed was ignored for this analysis, as flow in this region is typically at low speed and recirculatory in nature. The final fluid domain geometry is shown in Figure 16.

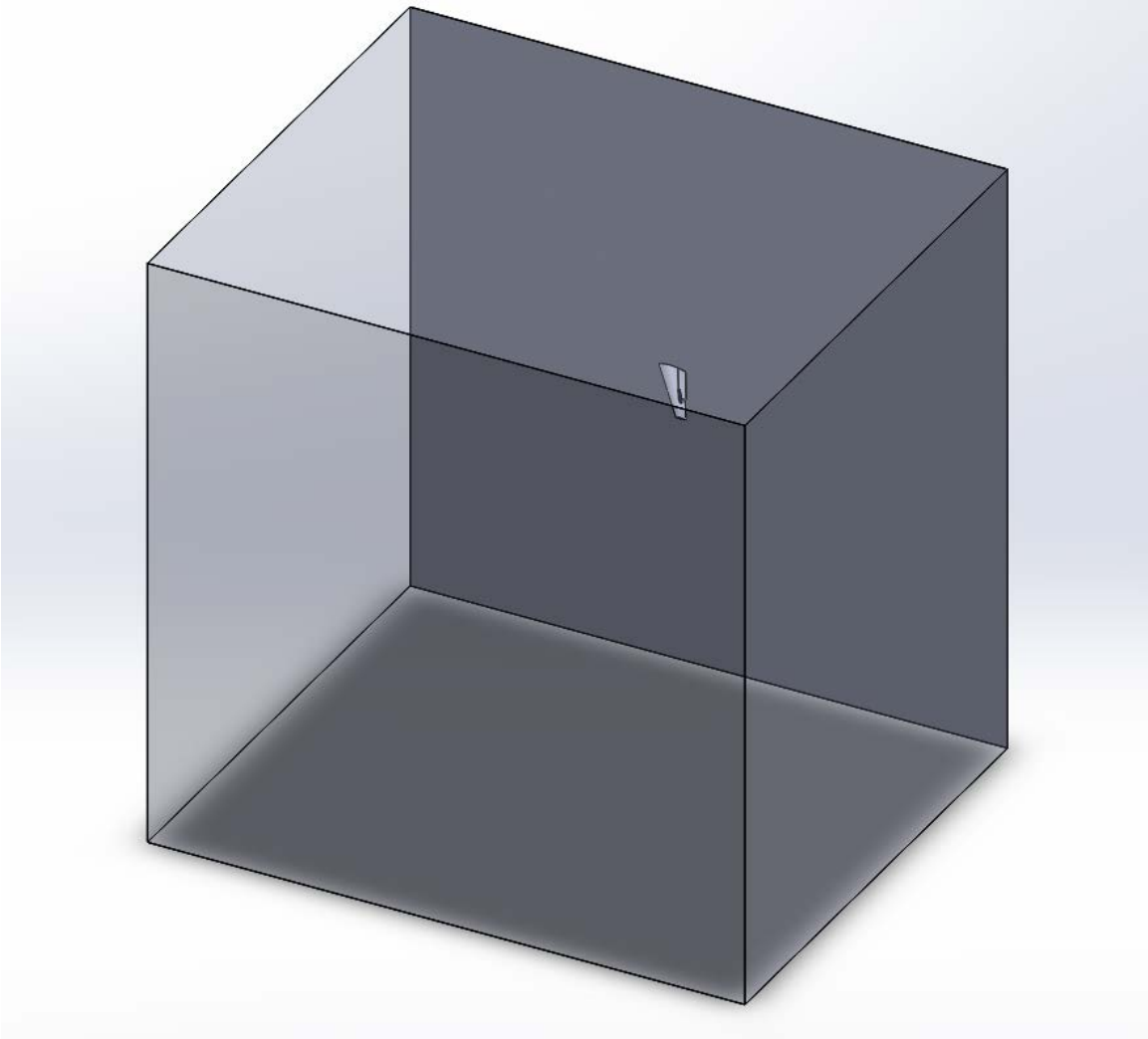

Figure 16. Full wing fluid domain

The cavity process was repeated for the three spoiler angles to be tested: 42° (fully deployed), 20°, and 0° (fully retracted). These geometries were then imported into the ANSYS Meshing tool.

B. MESH

1. General Mesh

The mesh was created using an automatic meshing method. An inflation layer was implemented to capture the boundary layer on the wing. The meshing tool was not able to create an inflation layer behind the spoiler. However, behind the spoiler the boundary layer

is separated and recirculatory, so the value of an inflation layer is diminished in this portion of the mesh. It is still important to ensure enough points are present in the area behind the spoiler to properly resolve the flow. This is especially true near the top edge of the spoiler, where a large shear flow may occur, causing large pressure and velocity gradients.

A face sizing restriction was enforced to ensure enough points were present on the surface of the wing, especially near the leading-edge stagnation point. At this point, the flow characteristics change quickly due to the rapid acceleration of the flow. The use of a curvature algorithm placed a greater concentration of points along the curve of the leading edge to capture the flow dynamics near the stagnation point.

2. Mesh Study

When meshing in 2-D, dense meshes can be created without considering RAM size compute time. This is not the case when meshing in 3-D, as mesh sides grow rapidly, taking significantly more memory and time to create. Thus, it is worthwhile to create mesh that is small enough to reduce memory space and compute time, without sacrificing solution accuracy. In order to confirm the quality of the mesh, several meshes of varying sizes were tested with the same initial conditions. The results of the mesh study are shown in Table 3.

Table 3. Mesh study results

Nodes	Lift [N]	Drag [N]	L/D	Cm
2 million	94.977	6.649	14.283	1.284
9 million	97.551	6.371	15.312	1.329
16.4 million	97.273	6.410	15.175	1.324

The meshes with 9 million and 16.4 million nodes produced similar results in all categories. The 9 million node mesh was chosen for calculation in order to reduce computational time, while still maintaining sufficient accuracy.

3. Mesh Verification

In addition to the mesh size study, qualitative methods were also used to confirm the ‘goodness’ of the mesh. First, the mesh was checked to ensure that it captured the boundary layer effects within the inflation layer by checking the y+ values, wall shear stress, and the velocity profile. A plot of the y+ value on the wing is seen in Figure 17, and x wall shear stress in Figure 18.

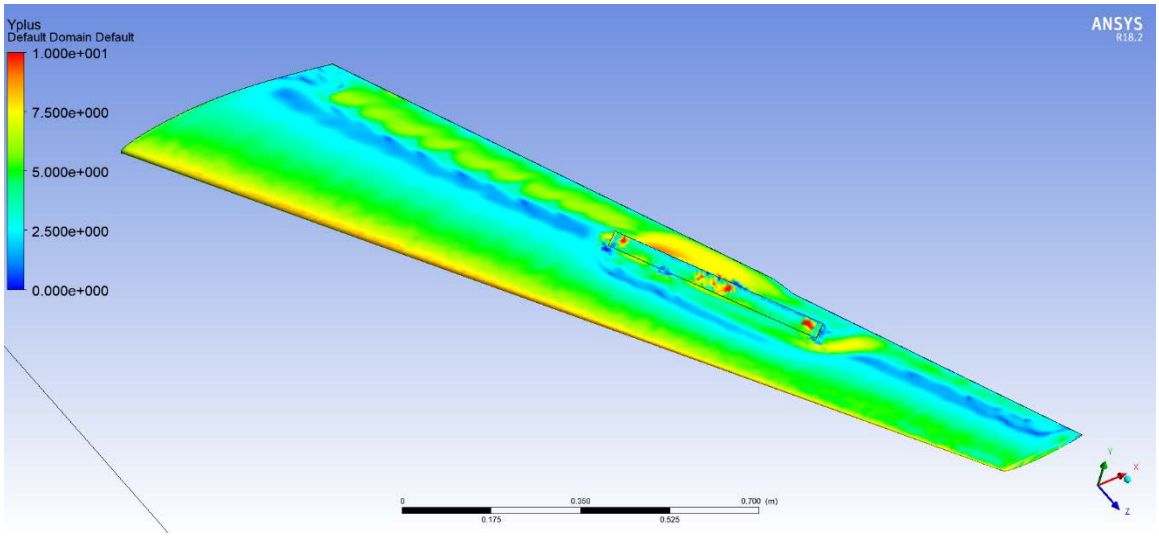

Figure 17. y+ values on the wing surface

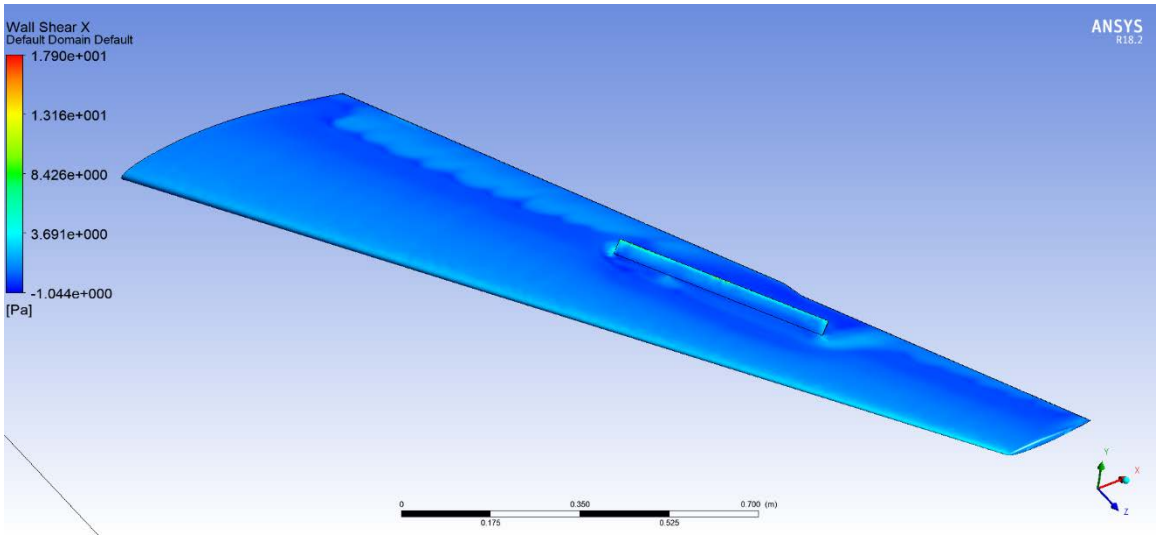

Figure 18. X wall shear stress on the wing surface

Based on Figure 18, transition does not occur until after separation of the flow, at about the ¾ chord. In this turbulent region, the y+ value is about 5. This particular mesh should be altered to have a thinner inflation layer in this turbulent region to lower the y+ value and better predict drag. Due to limited time and memory constraints, this study was unable to improve the mesh beyond this state, so the drag predictions based on this model are preliminary. Lift predictions are likely accurate, as lift is based more on pressure distribution than friction.

To visualize the boundary layer, first a plane was drawn parallel to the flow direction at the location of interest. The plane is colored to show the flow velocity. After creating the plane, the option to view mesh lines was selected. Then a line was drawn perpendicular to the wing surface in the same location of the plane. This line was used as a seed point for a set of vectors set to display the velocity. This setup is shown in Figure 19.

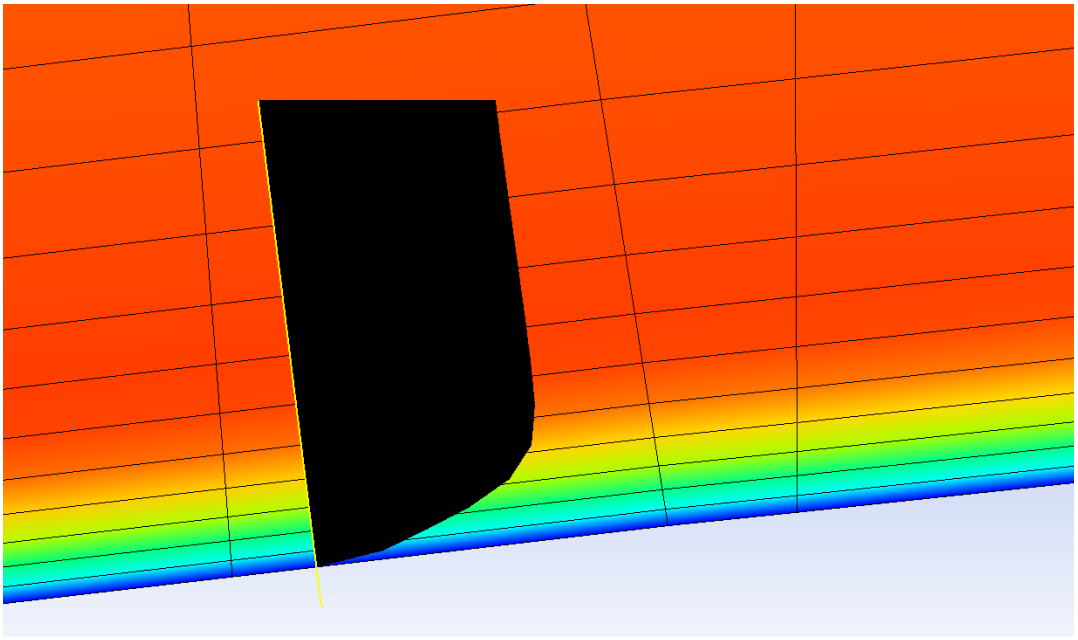

Figure 19. Boundary layer overlaid on mesh

The boundary layer profile (created by the vectors) is shown in black. The boundary layer extends to the point where the profile becomes constant. If this constant value is contained within the inflation layer, when combined with y+ values near 1 in the turbulent region, then it can be concluded that the mesh adequately captures the boundary layer dynamics.

The color of the plane can also be used to determine if the boundary layer is captured within the inflation layer of the mesh. The blue areas are slower and appear nearest to the wing boundary. This visually displays the no-slip condition on the wing surface. Traveling away from the wing, the flow speeds up and the colors go from blue to green to orange to red. This constant red color represents a constant flow velocity, indicating the end of the boundary layer. While this is not the free stream, it is far removed enough from the wing surface to be free of the viscous influence. Since this change to a constant color falls inside the inflation layer, it can again be concluded that the mesh captures the boundary layer effects.

4. Final Mesh

The final meshes for the three spoiler test cases are shown in Figure 20. Each mesh had the same characteristics within the ANSYS Meshing tool with regard to the inflation layer and element sizing around the wing. These values are shown in Appendix A.

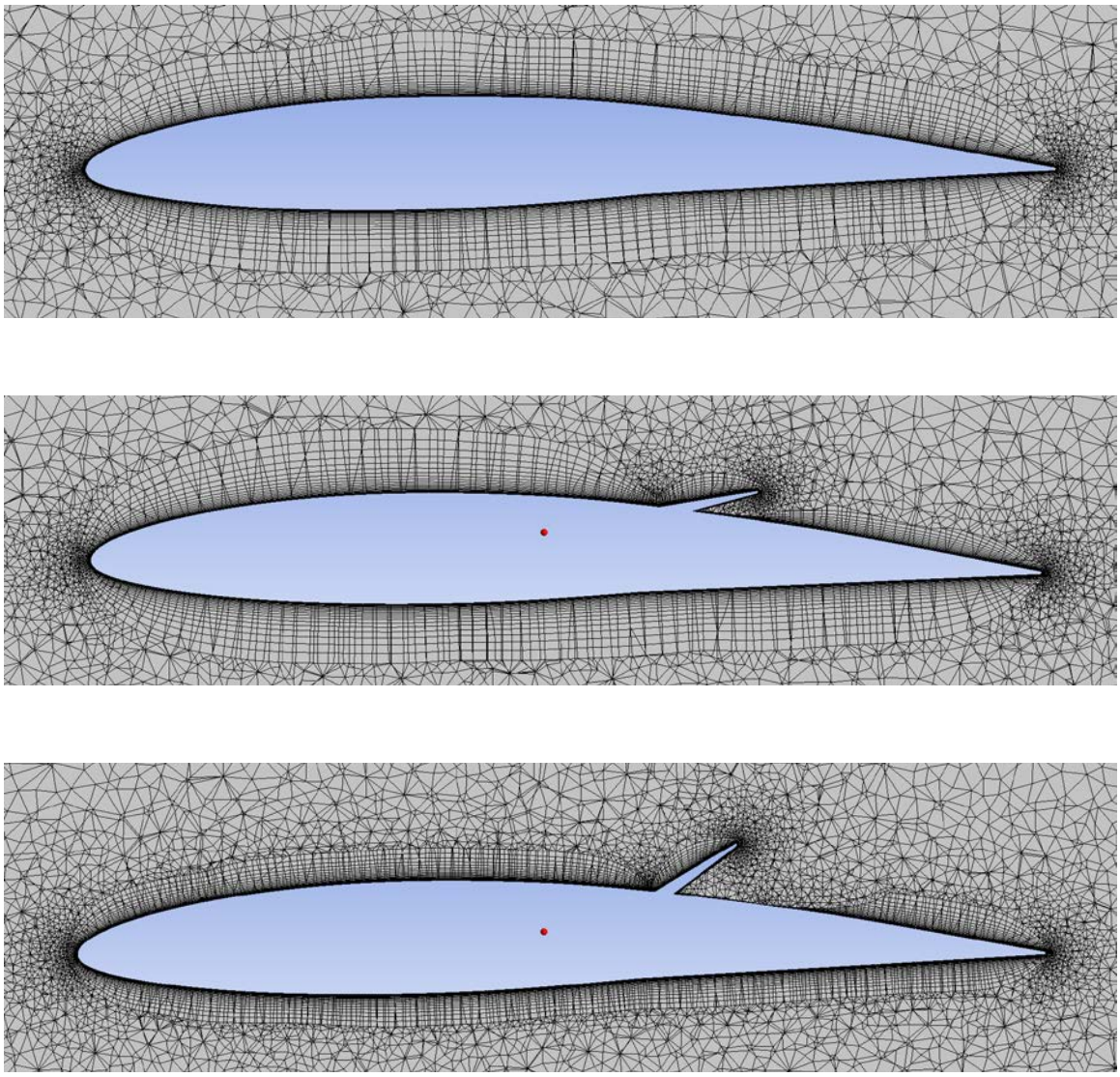

Figure 20. Final mesh renderings for spoiler at 0°, 20°, and 42°

C. SETUP

The boundary conditions were initialized similarly to the 2-D airfoil. Initial testing was done at 25 m/s flow velocity, but was later reduced to 19 m/s. This was determined to be a more accurate flight speed for the prototype based on the predicted weight of the model and the lift results from the initial tests at 25 m/s at the design AoA of 5° with spoiler down. Using the assumption that lift is proportional to the flow velocity squared, it was calculated that the wings would be able to lift the model flying at 19 m/s.

The front and bottom of the domain were made inputs with x-velocity and y-velocity initialized using the method outlined in Table 1. The back of the domain was set as an outlet, and the top and free side set as openings. The side to which the wing geometry is attached was initialized as a symmetry boundary, as the flow at this point is parallel to the boundary and flow is not expected to cross the boundary. An image of the boundary conditions is shown in Figure 21.

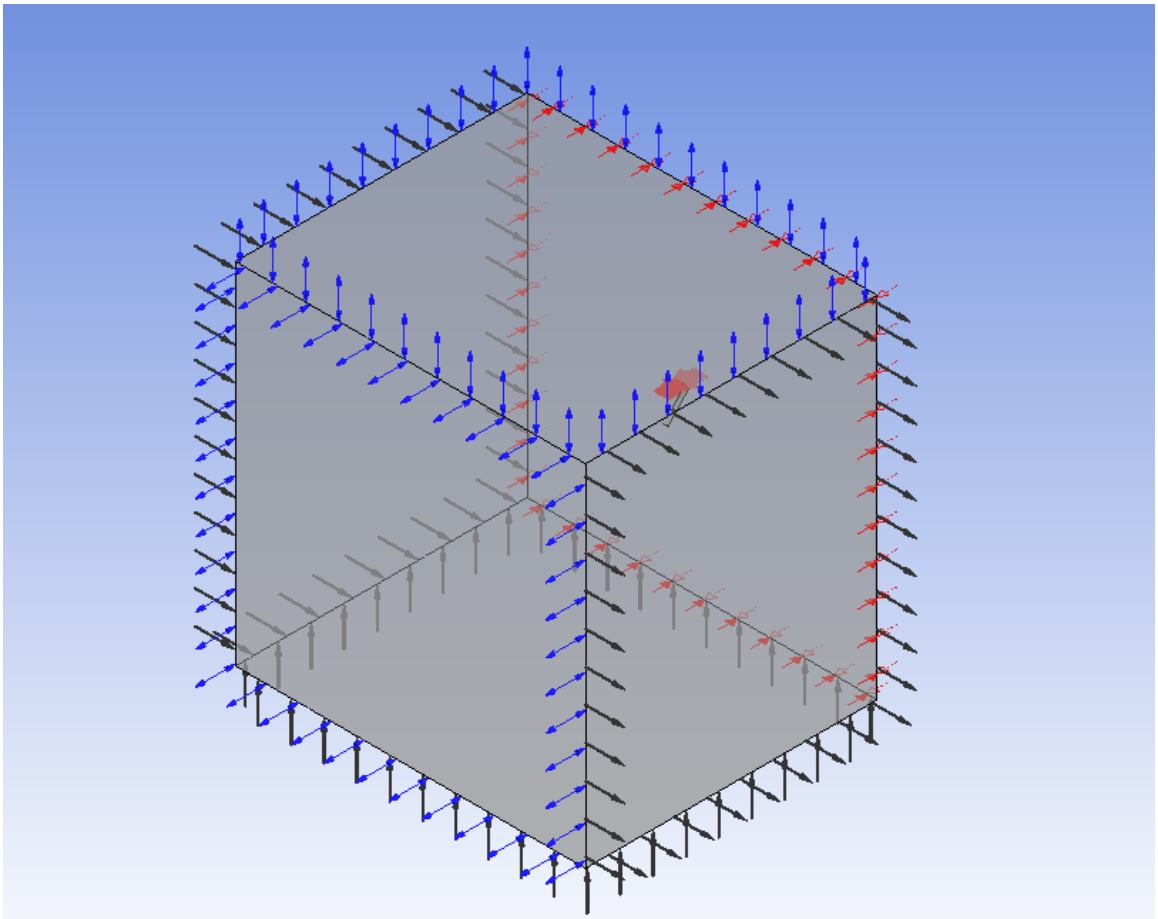

Figure 21. Full wing boundary conditions

Each spoiler angle was tested at AoA of 4°, 5°, and 6°, the most common flight angles for the model. When attached to the fuselage, the wing will have an inherent 5° AoA. The additional test angles were chosen to show variation of properties about the design point.

D. SOLUTION

After loading the setup file into the solver, the solution was iterated until the residuals reached a constant value (to within a small threshold). An example plot is shown in Figure 22.

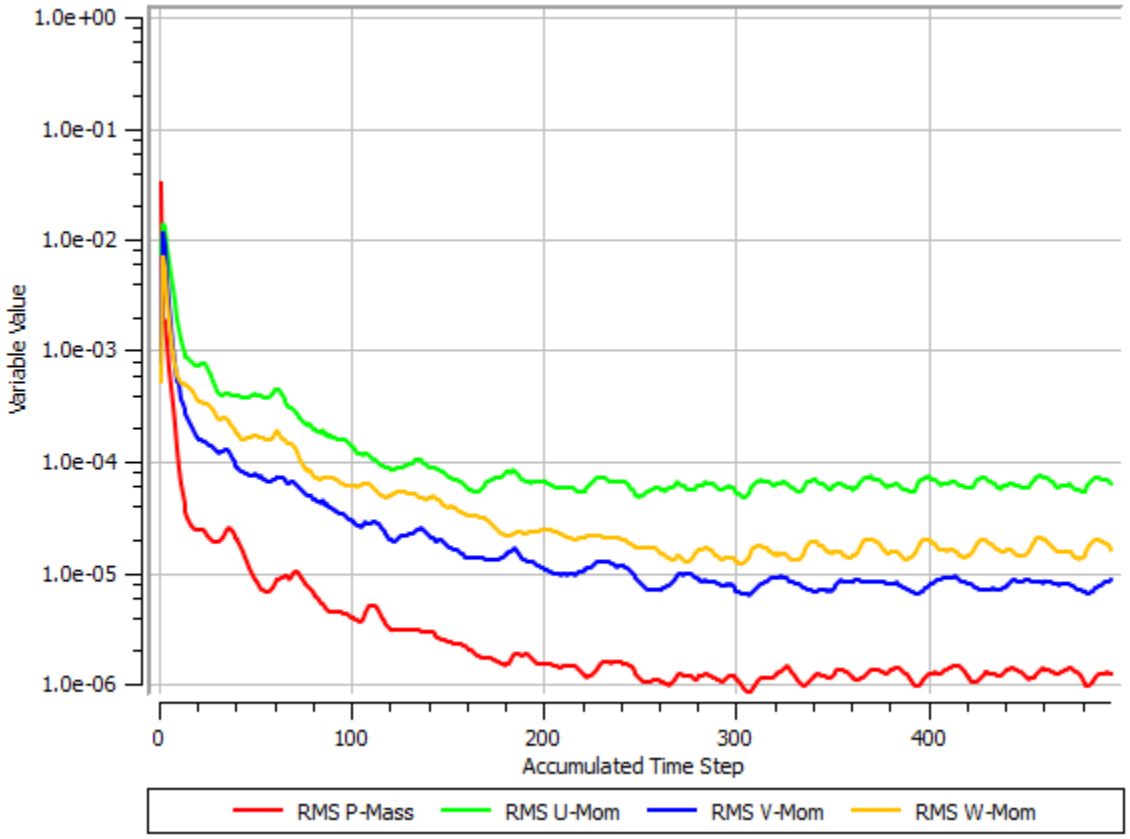

Figure 22. Example residual plot for 3-D calculation

V. ANALYSIS OF 3-D WING

A. LIFT, DRAG, MOMENT

The lift and drag and their associated coefficients were calculated using the same process as in Chapter II. The moment was again calculated using the torque value from the ANSYS function calculator. However, the point about which the torque was calculated was not located at the leading edge, but rather at the origin of the geometry.

First, the center of pressure (COP) is calculated by taking a weighted average of the total force on the wing. The formula for the x-component of the COP is shown in equation 9, with its equivalent in the ANSYS expression language in equation 10. These same expressions can be used to calculate the y- and z-components of the COP simply by substituting *y* or *z* for *x*. The COP is the point through which the lift acts.

$$x_{COP} = \frac{\sum Fx}{\sum F} \tag{9}$$

$$areaInt(X * (Pressure + Shear)) @ DefaultDomainDefault \,/\, areaInt(Pressure + Shear) @ DefaultDomainDefault \tag{10}$$

Knowing the COP, the moment about the z-axis can be transposed to the leading edge of the wing using equation 11 and the schematic in Figure 23.

$$M_{LE} = \frac{M_Z}{x_{COP}}(x_{COP} - x_{LE}) \tag{11}$$

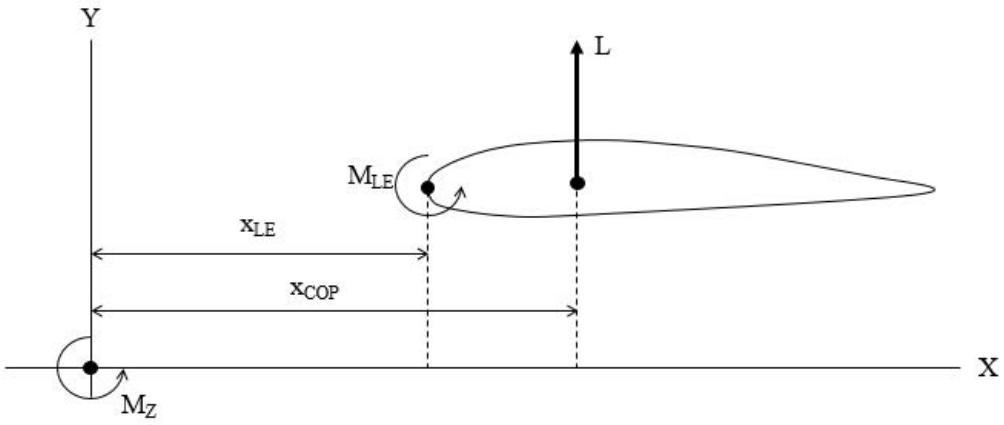

Figure 23. Transposition of pitching measured moment

Again, to calculate the pitching moment coefficient, the torque value is divided by the dynamic pressure and the chord. However, since the chord varies along the span of the wing, a representative chord must be determined, termed the mean aerodynamic chord.

The mean aerodynamic chord is calculated using a graphical method as shown in Figure 24. The chord length at the root is placed on either end of the tip chord, and vice versa [10]. In this calculation, the root chord is taken as if the taper was projected to the centerline [11]. Lines are drawn from the end of the root chords to the ends of the tip chords forming an “x”. The chord length at this intersection point is the mean aerodynamic chord. For this model the mean aerodynamic chord length was 0.4041 m.

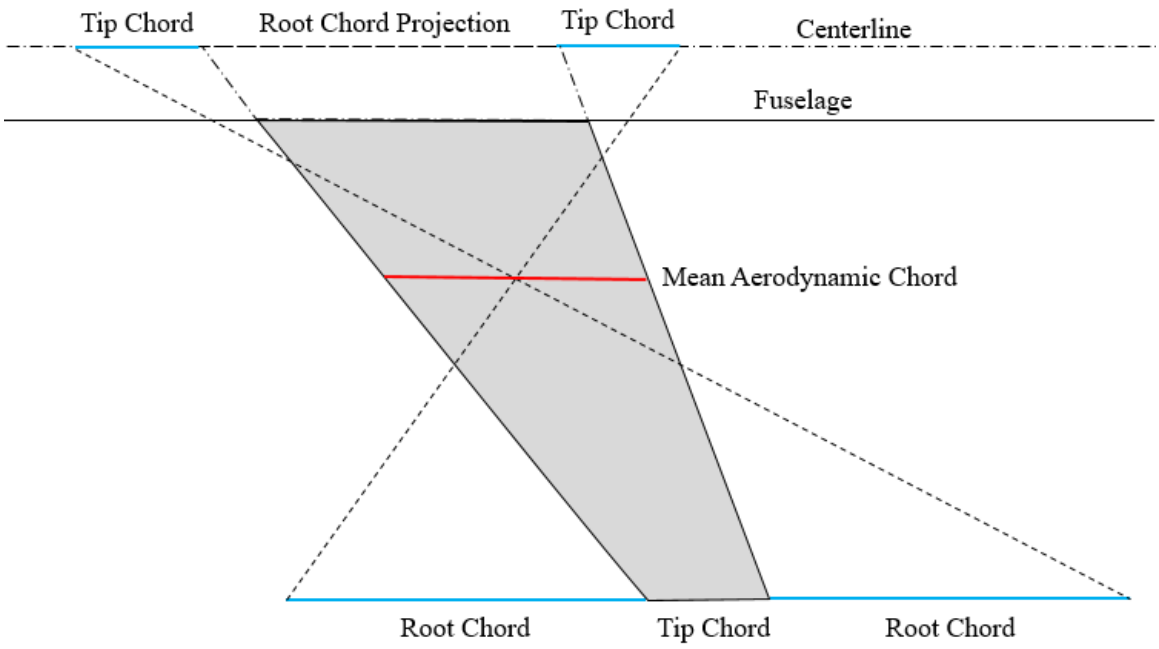

Figure 24. Graphical determination of mean aerodynamic chord.

B. EFFECT OF SPOILER ANGLE

1. Lift

Figure 25 shows the effect of the spoiler on the lift coefficient. As was expected, the lift increases with AoA, and decreases with greater spoiler angle. The decrease is linear with respect to AoA, as the three plotted lines are equally spaced. However, it is not linear with respect to the spoiler angle. The decrease from 0° spoiler to 20° spoiler is greater than from 20° to 42°. If the spoiler were to continue to be deployed, eventually a minimum lift coefficient would be reached. The beginning of this curve to asymptote can be seen in the plot.

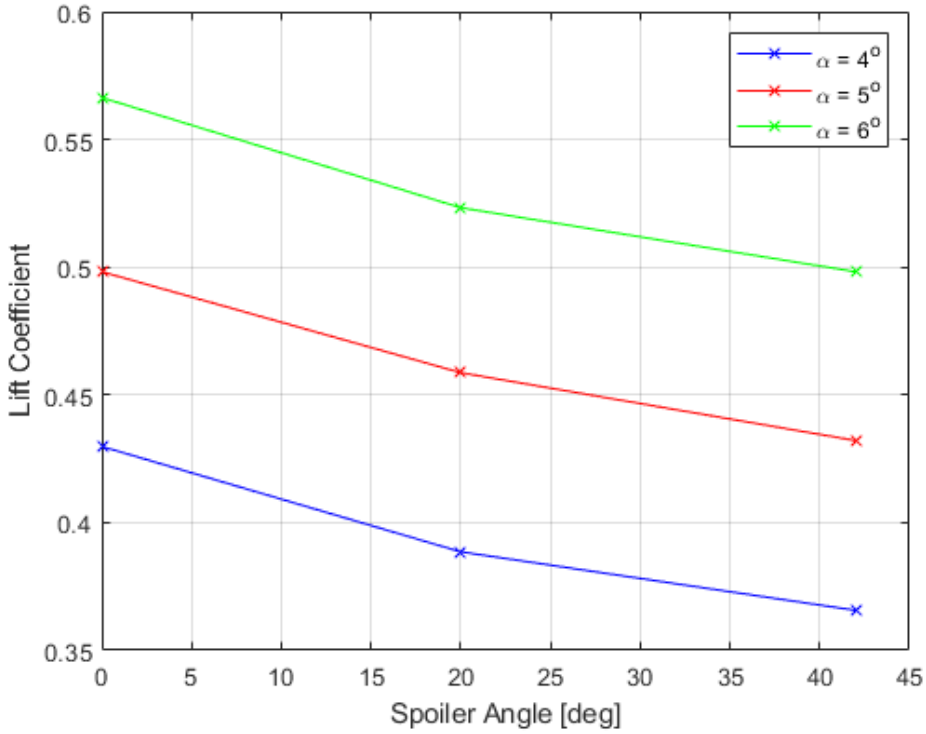

Figure 25. Lift coefficient vs. spoiler angle for AoA of 4°, 5°, and 6°.

The lift was modeled using a quadratic fit in the spoiler angle direction and linear fit in the AoA direction using the MATLAB 'ploy12' fit function. The fit is given in equation 12 with α is the AoA, and S is the spoiler angle. The r-square value for this regression was 0.9998.

$$C_L = 0.157 + 0.0683\alpha - 0.00227S - 4.79\times10^{-5}\alpha S + 2.23\times10^{-5}S^2 \qquad (12)$$

2. Drag

Figure 26 shows the effect of spoiler angle on the drag coefficient. Due to the y+ values of the calculation, drag values are not as accurate as desired. However, the trends displayed here likely will exist on a higher fidelity model.

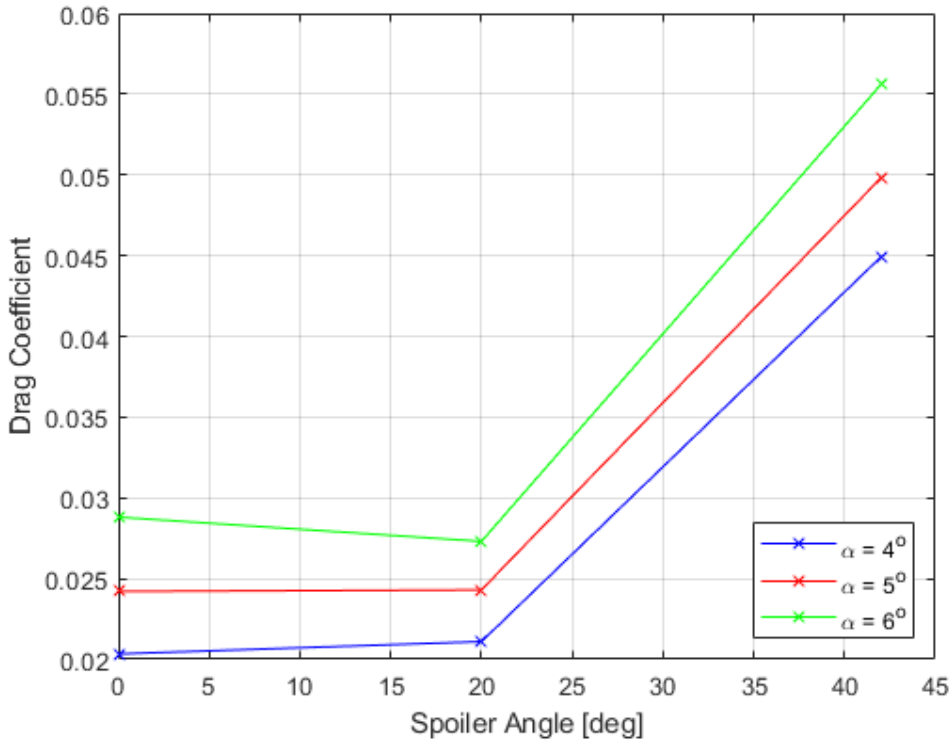

Figure 26. Drag coefficient vs. spoiler angle for AoA of 4°, 5°, and 6°.

The drag remains relatively constant as the spoiler angle is increased to 20°, but increases greatly moving from 20° to 42°. This large change in drag may be due to the fact that the 20° spoiler does not affect the flow as much as the fully extended spoiler. Velocity plots of the flow around the wing at the three spoiler angles are shown in Figure 27. These plots are taken near the center of the spoiler.

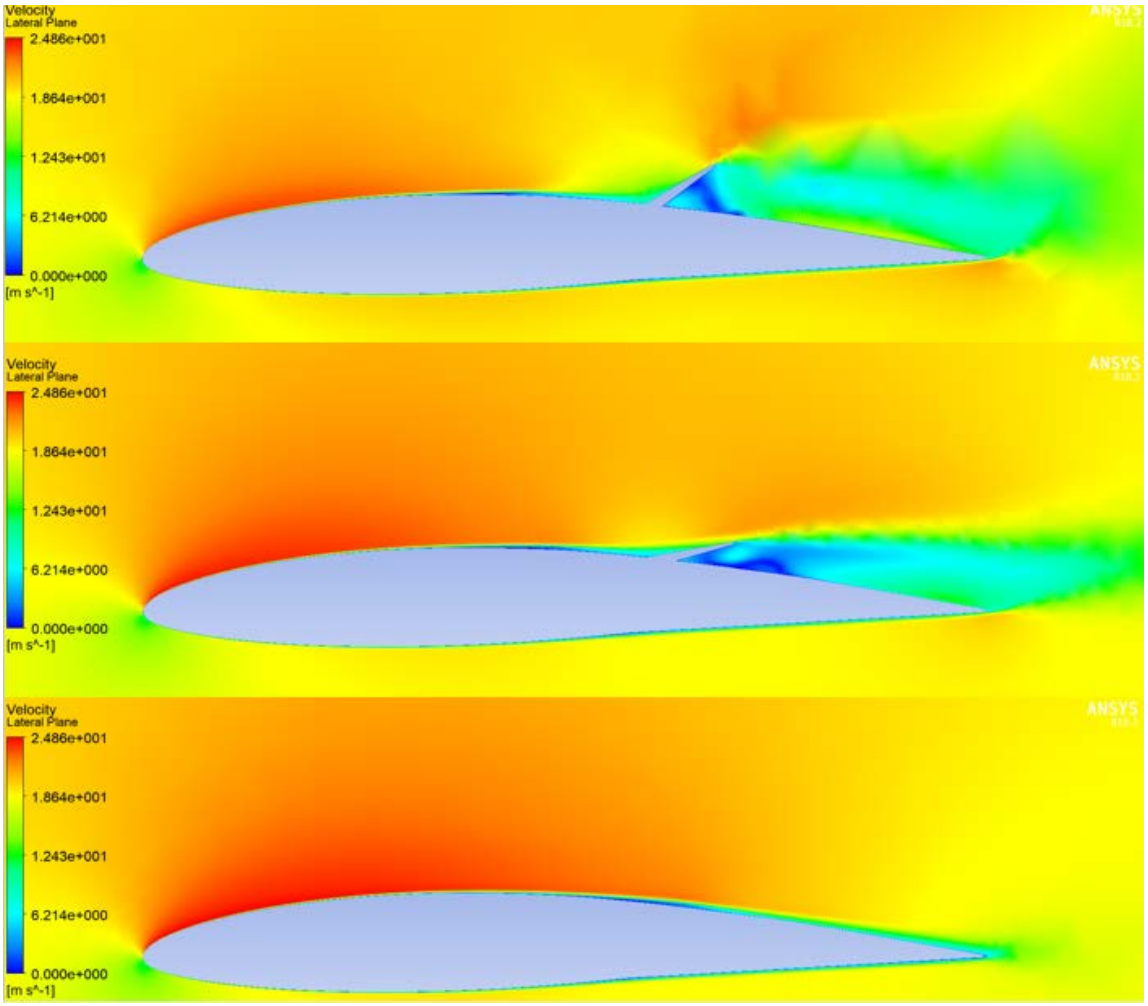

Figure 27. Velocity plots for spoiler angles of 42°, 20°, and 0° at inlet velocity of 19 m/s.

The boundary layer around the 20° spoiler does not seem to affect the flow as much as the 42° spoiler case. The 20° spoiler creates a bubble of slower moving air that sits in between the wing and the spoiler, but it does not bother the flow above it. The air flows from the high edge of the airfoil to the top of the spoiler. This is not the case for the 42° spoiler. The spoiler completely disrupts the flow, causing it to make a large turn, and creating a lot of vorticity in the flow, as indicated by the chaotic wake behind the spoiler. This vorticity can be linked to the large increase in drag on the wing. While this vorticity does exist in the 20° spoiler case, the wake is smaller, causing less drag.

This effect is also visible in the motion of the separation bubble, seen in blue on the upper surface of the wing. Separation bubbles form in adverse pressure gradients, as pressure rises moving in the direction of flow. As the spoiler angle increases, the separation bubble moves forward along the wing. The spoiler causes the flow to slow down, raising its pressure. This high-pressure region affects the flow forward of it, causing the pressure gradient to become more severe, and causing earlier separation. While separation causes less skin friction drag, it indicates greater pressure drag.

3. Pitching Moment

Figure 28 shows the effect of spoiler angle on the pitching moment coefficient about the leading edge of the root chord. As the spoiler angle is increased, the pitching moment decreases, indicating a lesser tendency for the nose to pitch down. This is caused by the loss of lift at increasing spoiler angle.

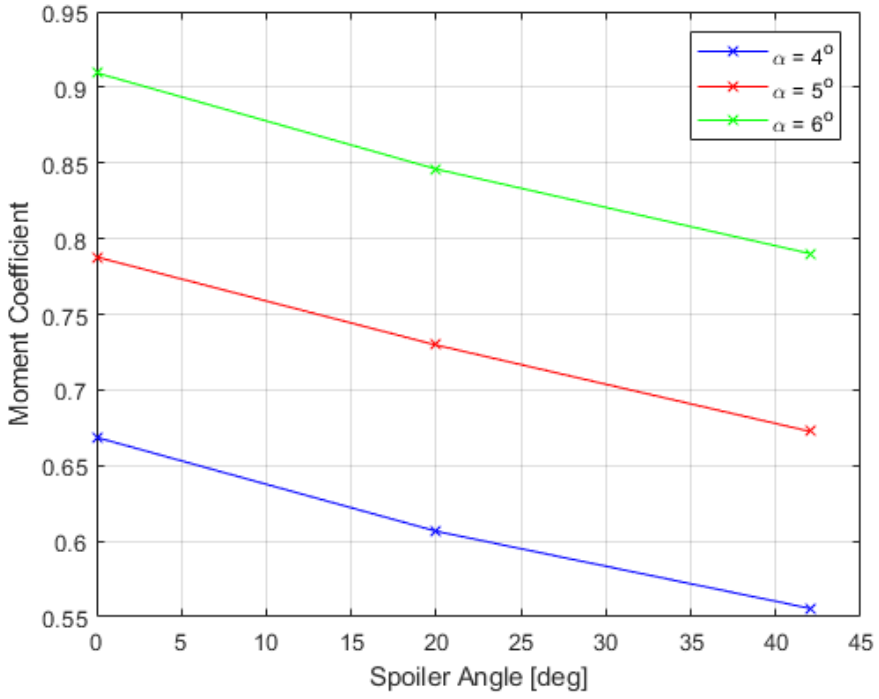

Figure 28. Drag coefficient vs. spoiler angle for AoA of 4°, 5°, and 6°.

4. Rolling Moment

On the B-52, the spoilers are used to control roll. Standard ailerons control roll by increasing lift on one wing and decreasing lift on the other simultaneously. Since the spoilers can only decrease lift, they are used individually to control roll. This roll ability is expressed using the rolling moment, a measure of the change in lift as it acts on the longitudinal axis of the aircraft. In this case, the moment is nondimensionalized by the dynamic pressure, planform area, and span. The span is used here instead of the chord as the rolling moment arm is based on where the lift acts along the span of the wing vice its position along the chord length. The rolling moment coefficient as a function of spoiler angle is shown in Figure 29.

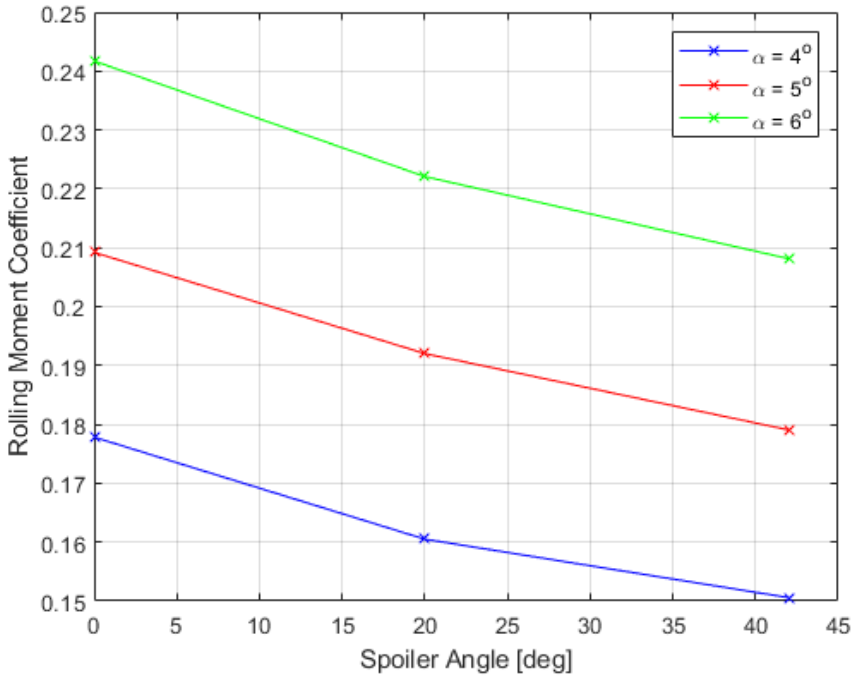

Figure 29. Rolling moment coefficient vs. spoiler angle for AoA of 4°, 5°, and 6°.

This plot is similar to the lift coefficient plot, as rolling moment is derived from lift. As the spoiler angle is increased, the rolling moment drops. However, this becomes

important when the spoilers are not used symmetrically. The wing with spoilers deployed will lose lift, and the greater lift on the opposite wing will cause the aircraft to roll. The difference in rolling moments caused by each wing will be the total rolling moment that the aircraft experiences, and can be used to calculate roll rate.

5. Yawing Moment

When using the spoilers unsymmetrically, a greater drag force is created by the spoiler that is deployed. This imbalance induces a yaw moment. Again, the moment is nondimensionalized by the dynamic pressure, planform area, and span. The yawing moment coefficient as a function of spoiler angle is shown in Figure 30.

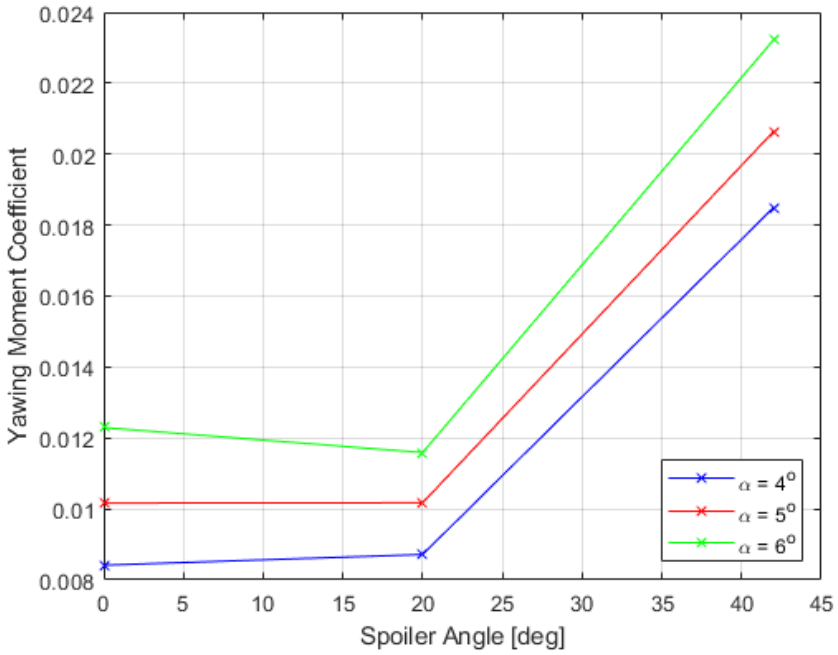

Figure 30. Yawing moment coefficient vs. spoiler angle for AoA of 4°, 5°, and 6°.

The yawing moment remains relatively constant as the spoiler angle is increased to 20°, but increases greatly moving from 20° to 42°. This plot is similar to the drag coefficient plot, as rolling moment is derived from drag. This also means that the yawing moment coefficients are not as accurate as desired.

The yawing moment becomes important when the spoilers are not used symmetrically. The wing with spoilers deployed will have greater yawing moment. The difference in yawing moments caused by each wing will be the total yawing moment that the aircraft experiences, and can be used to calculate yaw rate. This occurs at the same time as a change in roll when spoilers are used asymmetrically. The yaw induced will turn the aircraft in the same direction as the roll. This effect will keep the aircraft in coordinated flight. On the B-52, this effect is magnified due to the drag fingers on the spoilers.

6. Pressure Coefficient

The pressure coefficient at three spoiler angles is plotted in Figure 31. These plots are taken near the midpoint of the spoiler at 5° AoA.

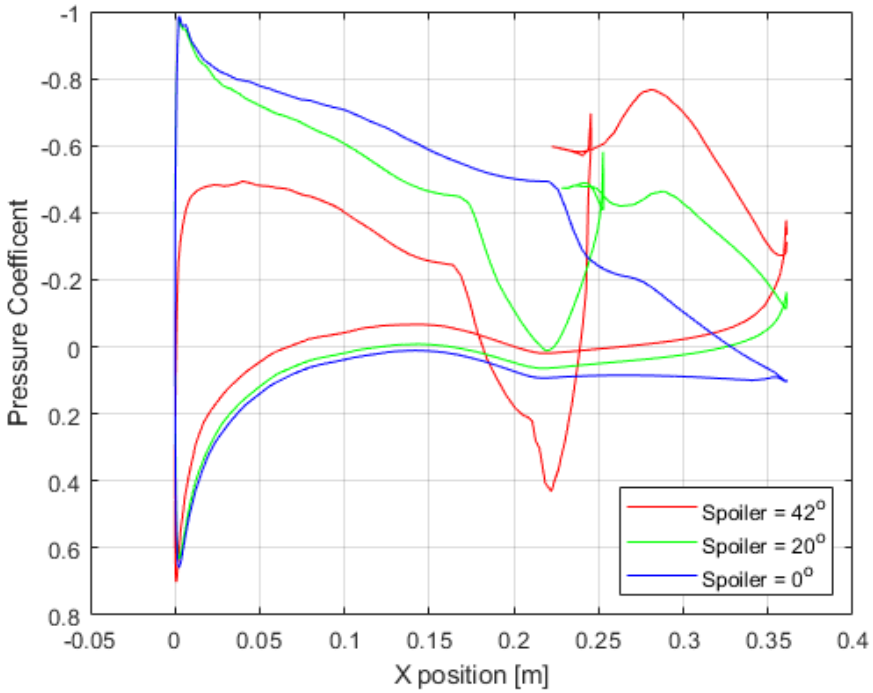

Figure 31. Pressure coefficient on the wing surface at 5° AoA.

Note the similarity between the blue line on this plot and that in Figure 9. As the spoiler angle increases, the pressure on the upper surface of the wing is affected greatly. In

the 20° spoiler angle case, the lift is mostly lost on the back side of the sing, downstream of the spoiler. When the spoiler is fully deployed, the effects are felt all the way at the leading edge, and the red line does not peak as high as the other test points.

As noted earlier, the integral of the pressure with respect to area yields the lift. Seen in Figure 25, as the spoiler angle increases, the lift decreases. This can be observed Figure 31 as well, albeit more subjectively. This effect is much more pronounced on the red 42° line, which in turn produces less lift.

7. X-Wall Shear Stress

The pressure coefficient at three spoiler angles is plotted in Figure 32. These plots are taken at the same location as those of the pressure coefficient.

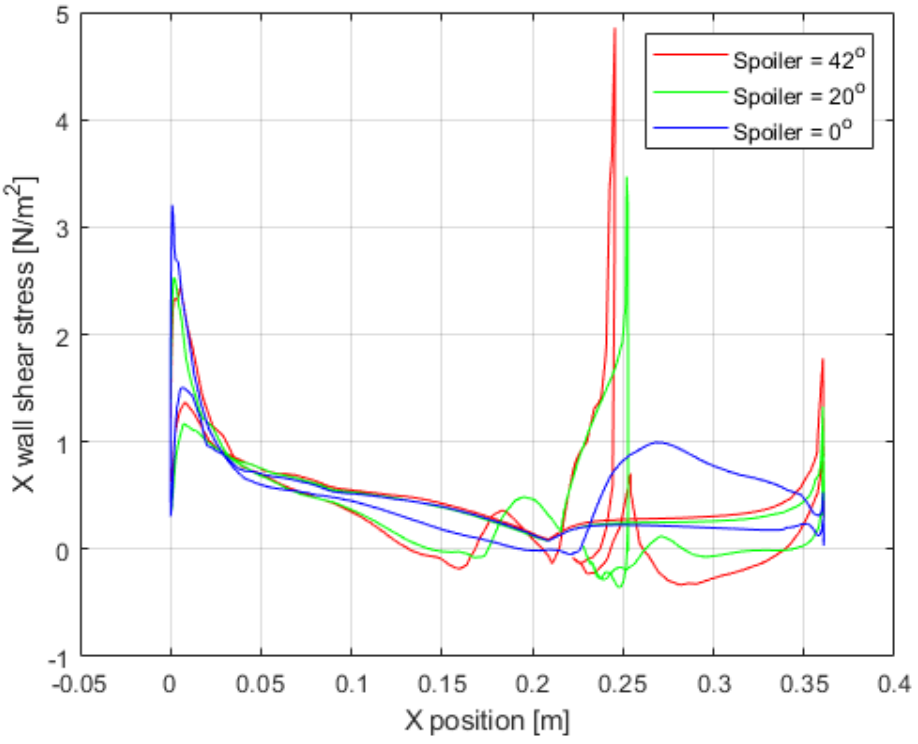

Figure 32. X wall shear stress on the wing surface at 5° AoA

Again, the blue line resembles the x-wall shear stress plot in Figure 10. In this plot we can observe the movement of the separation bubble from about 0.22 m with 0° spoiler to about 0.16 m with 42° spoiler. It is also notable that when the spoiler is not raised, the separation bubble forms at the location of the spoiler. However, this is most likely only coincidence, as the separation bubble will move based on flight speed and AoA.

VI. CONCLUSIONS AND FUTURE WORK

A. CONCLUSIONS

From the CFD analysis of the spoilers at low speeds, the spoiler was found to increase drag and decrease lift with increasing spoiler angle. The change in lift was able to be modeled using a polynomial fit. However, the drag was much less predictable; it remained relatively constant from a 0° spoiler angle to 20° spoiler angle, but grew sharply from 20° spoiler angle to 42° spoiler angle. This prediction of performance would be improved by testing more spoiler angles in between those tested in this thesis.

This thesis also provides a methodology for CFD testing. The process is described through building a fluid domain, creating and evaluating a mesh, inserting boundary conditions, and ensuring proper solution convergence.

B. FUTURE WORK

The next step of this project would be to further refine the mesh to improve the drag estimation. This should be followed by testing a greater range of spoiler angles, especially in the range between 20° and 42°. This would improve the fit of a regression model and better describe the non-linear characteristics of the wing spoiler.

In addition, wind tunnel testing of a wing section with a spoiler would provide a physical means of validating the results of the CFD study. This wing section need not be a scale replica of that tested in the CFD environment, only enough to provide a proof of concept.

THIS PAGE INTENTIONALLY LEFT BLANK

APPENDIX A. MESH CHARACTERISTIC VALUES

Table 4. Inflation layer characteristics of 2-D airfoil

Characteristic	Value
Inflation Method	First Layer Thickness
First Height Layer	1e-4 m
Maximum Layers	30
Growth Rate	1.1

Table 5. Edge sizing restriction characteristics of 2-D airfoil

Characteristic	Value
Element Size	5e-3 m
Growth Rate	1.2
Curvature Normal Angle	1.0°
Local Min Size	5e-4 m

Table 6. Inflation layer characteristics of 3-D wing

Characteristic	Value
Inflation Method	First Layer Thickness
First Height Layer	5e-4 m
Maximum Layers	20
Growth Rate	1.2

Table 7. Face sizing restriction characteristics of 3-D wing

Characteristic	Value
Element Size	5e-3 m
Size Function	Curvature
Growth Rate	1.2
Curvature Normal Angle	7.5°
Local Min Size	5e-4 m

THIS PAGE INTENTIONALLY LEFT BLANK

APPENDIX B. 2-D TEST RESULTS

Lift/Drag																				
chord	Area	U			C_L slope	C_L max														
[m]	[m^2]	m/s			0.02047	1.401839														
0.367206	0.000367	25																		
AoA-input	AoA-wing		x-Force	y-Force	z-torque	q	q*A	q*A*c	Drag	Lift	C_D	C_L	C_M	L/D						
[deg]	[deg]	[rad]	[N]	[N]	[N-m]	[Pa]	[N]	[N-m]	[N]	[N]	[]	[]	[]	[]						
-10	-5	-0.08727	-0.00595	-0.04093	-0.00088	370.317	0.135983	0.049934	0.001245	-0.04134	0.009155	-0.30404	-0.01758	-33.2118						
-9	-4	-0.06981	-0.00315	-0.02707	0.000376	370.317	0.135983	0.049934	0.001123	-0.02723	0.008255	-0.20022	0.007537	-24.2526						
-8	-3	-0.05236	-0.00082	-0.01336	0.001592	370.317	0.135983	0.049934	0.001046	-0.01335	0.00769	-0.09815	0.031879	-12.7637						
-7	-2	-0.03491	0.001022	-8.60E-05	0.002742	370.317	0.135983	0.049934	0.001025	3.93E-05	0.007539	0.000289	0.054915	0.03832						
-6	-1	-0.01745	0.002553	0.014916	0.004192	370.317	0.135983	0.049934	0.00098	0.015101	0.007208	0.11105	0.083946	15.4058						
-5	0	0	0.003534	0.028877	0.005358	370.317	0.135983	0.049934	0.001004	0.029075	0.00738	0.213811	0.107312	28.97146						
0	5	0.087266	0.001511	0.103762	1.24E-02	370.317	0.135983	0.049934	0.001511	0.103762	0.011111	0.763054	0.247691	68.67835						
5	10	0.174533	-0.01019	0.159317	0.016581	370.317	0.135983	0.049934	0.003737	0.159599	0.02748	1.17367	0.332051	42.71046						
8	13	0.226893	-0.01996	0.184639	0.018363	370.317	0.135983	0.049934	0.005934	0.18562	0.043637	1.365026	0.367745	31.28172						
9	14	0.244346	-0.02285	0.189382	0.01867	370.317	0.135983	0.049934	0.007053	0.190626	0.051869	1.401839	0.373889	27.02627						
10	15	0.261799	-0.02485	0.190417	0.018718	370.317	0.135983	0.049934	0.008597	0.191839	0.063224	1.410759	0.374864	22.31349						
11	16	0.279253	-0.02555	0.187731	0.018563	370.317	0.135983	0.049934	0.010739	0.189157	0.078972	1.391041	0.371748	17.61435						
15	20	0.349066	0.010868	0.140393	0.019778	370.317	0.135983	0.049934	0.046834	0.132796	0.344412	0.97657	0.396076	2.835472						

THIS PAGE INTENTIONALLY LEFT BLANK

APPENDIX C. 3-D TEST RESULTS

Lift/Drag													
chord	Area	U	span						C_L slope	C_L max			
[m]	[m^2]	[m/s]	[m]						0.22852	0			
0.4041	0.5732	19	1.476										
					pitch								
Spoiler Ar	AoA		x-Force	y-Force	z-moment	xCOP	zCOP	q	q*A	q*A*c	q*A*s	Drag	Lift
[deg]	[deg]	[rad]	[N]	[N]	[N-m]	[m]	[m]	[Pa]	[N]	[N-m]	[N-m]	[N]	[N]
0	4	0.069813	-1.18887	52.7416	302.806	5.5931	0.610682	213.894	122.604	49.54429	180.9636	2.493094	52.69606
20	4	0.069813	-0.74254	47.7034	270.933	5.60238	0.609694	213.895	122.6046	49.54452	180.9644	2.586891	47.63899
42	4	0.069813	2.3655	45.1072	237.674	5.63234	0.607821	213.9	122.6075	49.54568	180.9686	5.506257	44.83231
0	5	0.087266	-2.36712	61.1081	356.632	5.59344	0.619813	213.9	122.6075	49.54568	180.9686	2.967809	61.08187
20	5	0.087266	-1.93362	56.2882	326.077	5.60207	0.617924	213.917	122.6172	49.54962	180.983	2.979578	56.24253
42	5	0.087266	1.46538	53.3117	288.879	5.62946	0.61161	213.899	122.6069	49.54545	180.9678	6.106225	52.98112
0	6	0.10472	-3.74592	69.4301	411.412	5.59394	0.629907	213.901	122.6081	49.54591	180.9695	3.532022	69.44131
20	6	0.10472	-3.3767	64.1541	378.598	5.60105	0.626466	213.9	122.6075	49.54568	180.9686	3.347727	64.15562
42	6	0.10472	0.392527	61.4595	340.81	5.62648	0.616676	213.9	122.6075	49.54568	180.9686	6.814644	61.08179
About LE					About root		About root						
Moment	C_D	C_L	C_M	L/D	Roll Mom	C_roll	Yaw Mom	C_yaw					
[N-m]	[]	[]	[]	[]	[N-m]	[]	[N-m]	[]					
32.10996	0.020335	0.429807	0.648106	21.13681	32.18053	0.177829	1.522488	0.008413					
29.1313	0.021099	0.388558	0.587982	18.41554	29.04521	0.160502	1.577212	0.008716					
26.68354	0.04491	0.365657	0.538564	8.142067	27.25002	0.150579	3.346819	0.018494					
37.83713	0.024206	0.49819	0.763682	20.58147	37.85934	0.209204	1.839487	0.010165					
35.0444	0.0243	0.458684	0.707259	18.87601	34.75361	0.192027	1.841153	0.010173					
32.3011	0.049803	0.432122	0.651949	8.676575	32.40378	0.179058	3.734628	0.020637					
43.68192	0.028807	0.566368	0.881645	19.6605	43.74157	0.241707	2.224846	0.012294					
40.62744	0.027304	0.52326	0.82	19.16393	40.19131	0.22209	2.097237	0.011589					
37.94746	0.055581	0.49819	0.765909	8.963313	37.66767	0.208145	4.202427	0.023222					

THIS PAGE INTENTIONALLY LEFT BLANK

LIST OF REFERENCES

[1] B. Hogin, “Control and In-Flight Diagnostic of B-52 Type Aircraft,” M.S. thesis, Dept. Mech. and Aerospace Eng., NPS, Monterey, CA, 2020.

[2] U.S. Air Force, “B-52H Stratofortress fact sheet,” Dec. 16, 2015. [Online]. Available: https://www.af.mil/About-Us/Fact-Sheets/Display/Article/104465/b-52-stratofortress/.

[3] F. Hitchens, The Encyclopedia of Aerodynamics. United Kingdom: Andrews UK Limited, 2015.

[4] L. Loftin, Quest for Performance: The Evolution of Modern Aircraft. United States: NASA, 2012.

[5] ANSYS. Cannonsburg, PA, USA. 2011. “ANSYS CFX-Solver Theory Guide.” [Online] Available: http://read.pudn.com/downloads500/ebook/2077964/cfx_thry.pdf

[6] K. Jones, email, Aug. 2019.

[7] F. White, Viscous Fluid Flow, 3rd ed. New York, NY, USA: McGraw-Hill, 2006.

[8] K. Jones, email, Jan. 2020.

[9] “B-52, The ‘StratoFortress.’” Virginia Tech, [Online]. Available: http://www.dept.aoe.vt.edu/~mason/Mason_f/B52S05.pdf.

[10] P. Johnson, “Mean aerodynamic chord,” 2003, [Online]. Available: https://www.airfieldmodels.com/information_source/math_and_science_of_model_aircraft/formulas/mean_aerodynamic_chord.htm.

[11] D. Scholz, “Aircraft design lecture notes,” Hamburg University of Applied Sciences, 2015, [Online]. Available: https://www.fzt.haw-hamburg.de/pers/Scholz/HOOU/.

THIS PAGE INTENTIONALLY LEFT BLANK

INITIAL DISTRIBUTION LIST

1. Defense Technical Information Center
   Ft. Belvoir, Virginia

2. Dudley Knox Library
   Naval Postgraduate School
   Monterey, California